NACA

RESEARCH MEMORANDUM

AERODYNAMIC CHARACTERISTICS INCLUDING SCALE EFFECT OF SEVERAL WINGS AND BODIES ALONE AND IN COMBINATION AT A MACH NUMBER OF 1.53

By

Milton D. Van Dyke

Ames Aeronautical Laboratory
Moffett Field, Calif.

NATIONAL ADVISORY COMMITTEE FOR AERONAUTICS

WASHINGTON

December 20, 1946

NATIONAL ADVISORY COMMITTEE FOR AERONAUTICS

RESEARCH MEMORANDUM

AERODYNAMIC CHARACTERISTICS INCLUDING SCALE EFFECT OF SEVERAL WINGS AND BODIES ALONE AND IN COMBINATION AT A MACH NUMBER OF 1.53

By Milton D. Van Dyke

SUMMARY

An investigation was conducted to evaluate the interaction of wing and body at supersonic speed. Three wing models of straight and sweptback plan form and three related bodies of revolution were tested separately and in all possible wing-body combinations. Lift, drag, and pitching moment were measured at 1.53 Mach number through a range of Reynolds numbers. The results of the investigation and a discussion of the experimental technique are presented.

Up to the limits of the investigation, the aerodynamic characteristics of the models tested were found to be, for the wings, independent of scale beyond one-half million Reynolds number (based on mean geometric chord), and, for the sharp-nose bodies, nearly independent of scale beyond Reynolds numbers of three or four millions (based on length). Beyond these values, the supersonic aerodynamic characteristics of the models tested can, with a few exceptions, be closely predicted whenever

theory exists.

It was found that the effect of interaction is such that the portion of wing area blanketed by the body should be considered completely effective aerodynamically in estimating the lift and drag of a combination. This rule probably fails if the wing is close to the base of the body, or if the wing span is small compared with the body diameter.

INTRODUCTION

The problem of estimating the interaction between simple aerodynamic shapes in combination has, at subsonic speeds, been the subject of both theoretical and experimental investigation. This same problem at supersonic speeds now confronts both the aircraft designer, who must combine the characteristics of separate aircraft elements, and the wind-tunnel investigator, who must know to what extent he is justified in breaking down a general research investigation into studies of individual components.

Existing supersonic theory permits the prediction, at least approximately, of the aerodynamic characteristics of certain simple shapes such as rectangular wings and pointed bodies of revolution. The limited amount of experimental evidence now available confirms, with certain exceptions, the validity of present theory. However, no theory treating combinations of these basic forms has yet been advanced, and virtually no experimental results illuminate this problem.

An example of the consequent state of ignorance is the current uncertainty as to whether the area of wing blanketed by the body should be considered in estimating the supersonic performance of a wing-body combination, as is common in the subsonic case.

To provide information on the interaction of wings and bodies at supersonic speeds was the aim of the present investigation. Measurements were made at 1.53 Mach number of the lift, drag, and pitching-moment characteristics of several wings and bodies and the resulting combinations. Models were chosen to bring out possible variations of aerodynamic characteristics resulting from modifications of wing plan form or of body contour. Moreover, the models were chosen similar to possible designs of supersonic aircraft so that the results might be of direct application. Variation of tunnel pressure provided a range of test Reynolds numbers to give an insight into the effects of scale.

In the present report, the results for the wings and bodies of revolution alone are first analyzed in comparison with existing theory. Following that, the effect of combining these basic forms is discussed, and simple empirical rules are derived for estimating the characteristics of a combination from those of its components. An attempt is made to explain the physical basis for these rules, and certain limitations to their validity are suggested.

APPARATUS AND METHODS

Tunnel

The investigation was conducted in the Ames 1- by 3-foot supersonic wind tunnel No. 1. This is a variable-pressure tunnel fitted temporarily with a fixed two-dimensional-flow nozzle designed to provide a uniform Mach number of 1.5 in a 1- by $2\frac{1}{2}$-foot rectangular test section.

The tunnel is powered by synchronous electric motors which drive four three-stage centrifugal compressors at a maximum rated load of 10,000 horsepower in continuous operation. The level of total pressure in the tunnel can be maintained automatically at any selected value from a minimum of 2 pounds per square inch to a maximum, at the present Mach number, of 25 pounds per square inch. Humidity of the air can be reduced to a low value by repeatedly evacuating the tunnel and refilling it with dry air from a supply tank.

Instrumentation

Lift, drag, and pitching moment of three-dimensional models are measured by an electric strain-gage balance. Figure 1 shows the general arrangement of the balance inside the tunnel test section. Figure 2 is a schematic drawing of the balance mechanism. A beam carrying the model on a sting is mounted inside a housing that is supported by a strut spanning the tunnel downstream of the test section. Five

constant-stress cantilever springs constrain the streamwise and vertical motion of the beam relative to the housing. Additional restraints limit its rolling and transverse movement. Each of the five springs carries four strain-gage windings which are connected in a Wheatstone-bridge circuit, and a constant electromotive force from a direct current power supply is impressed upon the circuit. Under static conditions each circuit is electrically balanced. Aeroydnamic forces transmitted from the model to the spring unbalance the circuit, and the amount of unbalance is measured on a light-beam galvanometer. The galvanometer readings are directly proportional to the forces, the constants of proportionality being determined by static calibration.

A single strain-gage unit measures the component of force parallel to the beam while readings of the other two pairs of units are combined electrically to give the force perpendicular to the beam and the pitching moment acting about an arbitrarily fixed point. From these three quantities the lift, drag, and pitching moment acting on the model are calculated. The beam is electrically insulated from the housing, and fouling between the beam and the rest of the balance is indicated by an ohmmeter. The forward section of the housing which contains the balance beam can be rotated through $\pm 5^{\circ}$ in pitch to vary the angle of attack of the model. The pivot is behind the model, so that angle-of-attack changes involve vertical displacement of the model,

as shown in figure 1.

The sting supporting the model is completely enclosed by a shroud that extends from the front of the balance housing to within 1/32-inch of the model base. Shrouding serves primarily to eliminate all aerodynamic tare forces upon the sting. Furthermore, the entire interior of the balance is maintained at the base pressure of the model, so that base pressure readings can be obtained simply by measuring the pressure inside the housing.

The tunnel test section is fitted with 1-1/4-inch thick, 18-inch-diameter optically ground plate-glass windows. A schlieren apparatus permits observation of the flow field about the models. The system consists of a light source, two 18-inch-diameter spherical mirrors of 120-inch focal length, an adjustable knife edge, and a combination camera and viewing screen. A 1000-watt high-pressure mercury-vapor lamp provides either continuous illumination for visual observation or a single intense flash of approximately 6 microseconds duration for high-speed photography.

Pressure measurements required in reducing the force data to coefficient form are observed on a multiple-tube mercury manometer. Included are the total pressure upstream of the test section, which is used in computing dynamic pressure, and the static pressures at the test section and inside the balance, both of which enter into base drag calculations.

Specific humidity of the air in the tunnel is determined

by using a standard Bureau of Mines dewpoint apparatus. In this device a stream of the sample air is directed against a polished metal mirror which is cooled by evaporation of bottled carbon dioxide. Readings are made of the pressure and temperature at which formation of dew commences at the center of the mirror. When the tunnel total pressure is less than atmospheric, tunnel air is drawn through the dewpoint apparatus by a vacuum pump.

Models

A photograph of the wings and bodies investigated is shown in figure 3. All pertinent dimensions of the models are given in figure 4.

Three related bodies of revolution were investigated. These are referred to as the "basic," the "blunt," and the "bulbous" bodies. As the names suggest, the latter two shapes represent modifications of the first. The basic body had a sharp conical nose of 20° semiangle followed by an ogival transition to a cylindrical midportion. It was moderately boat-tailed, and had an over-all fineness ratio of seven. The blunt body was identical with the basic body, except that the pointed nose was rounded off to a 1/8-inch radius. This was done to ascertain the possible effects of a strong bow wave intersecting the wing of a combination. The bulbous body had the same ogival head as the basic body, but the rear portion was undercut. This was done to ascertain

the possible effects of pronounced body curvature at the wing root of a combination. The bodies were carefully machined from steel and highly polished. They were built up of two pieces plus a filler plate, as shown in figure 3.

Two wing plan forms were investigated. These are referred to as the "straight" and the "sweptback" plan forms. Both had a taper ratio of two to one, an aspect ratio of four, and the same area. The sweptback plan form can be visualized as being derived from the straight plan form by shearing in the streamwise direction until the midchord line has been rotated through 35°. The leading edge is then swept back approximately 41° and, at the Mach number of this investigation, lies ahead of the Mach cone springing from its apex. Wing tips were cut off parallel to the flight direction.

It was anticipated that this investigation might show the portion of wing area blanketed by a body to be only partially effective aerodynamically. Thus it was expected that when these bodies and wings were combined, the combination might carry lift and drag forces smaller than the sums of the forces on its components. The extent of this possible ineffectiveness could be determined experimentally by testing in combination another wing model which has the effect of adding the original plan form entirely outside - rather than through - the bodies. This was done only with the straight plan form and, to simplify the model, in combination only with the basic and blunt bodies.

Accordingly three wing models were constructed: one each of straight and sweptback plan form, and a third, comprising the straight plan form divided at its center by the maximum body diameter, to be tested only in combination. All three wings were of 5-percent-thick section in the streamwise direction. In all cases an isosceles triangular profile was chosen for the wings. This is a representative section known to have good aerodynamic characteristics at supersonic speeds and, in addition, was easy to construct. Angles of attack are referred to the flat lower surface. The models were machined from heat-treated tool steel. Leading and trailing edges were ground to a thickness of less than 0.002 inch.

When tested alone, the first two wings were clamped in a small conical fitting, shown in figure 3, which was mounted at the end of a sting. To form a wing-body combination, the filler plate of the bodies was removed and replaced by any one of the wings. When assembled, the wing was at zero angle of incidence with respect to the axis of the body. Three typical wing-body combinations are sketched in figure 5. All screw holes and gaps were filled with beeswax and finished smooth prior to testing. Sting lengths for the models were so chosen that a wing, when tested in combination, occupied the same streamwise location in the test section as when tested alone.

In order to increase the range of positive angles of attack, all models were set on their stings at an initial angle of 3°. The available balance range of $\pm 5^\circ$ then

provided nominal angles of attack for models of from -2 to 8°. Photographs of typical model installations are shown in figure 6.

Tunnel Calibration

Certain results obtained in calibrating the tunnel are essential to an understanding of the investigation. They will be mentioned here insofar as they concern the present tests.

Chief among these results is the determination of the effect of humidity. It has been found that the quantities associated with the flow in the test section - total pressure, static pressure, dynamic pressure, and Mach number - vary with the amount of moisture in the stream. Values of the aerodynamic coefficients of models tested, however, appear to be independent of humidity below a value of approximately 0.0014 pound of water per pound of air provided the variation of the flow quantities is taken into account in the reduction of the data. The specific humidity was maintained below 0.0008 in the present investigation.

The Mach number in the test section, in addition to varying with humidity, was found in the calibration to depend slightly upon tunnel total pressure. In this investigation, the Mach number at the position of the wings varied because of the combined effects of humidity and tunnel pressure between extremes of 1.525 and 1.545, lying ordinarily close to 1.530.

The streamwise static-pressure gradient in the test section amounts to $1\frac{1}{2}$ percent of the dynamic pressure over the

length of the bodies. The corresponding correction to drag, estimated as a simple buoyancy effect, is negligible in every case. The pressure gradient across the tunnel was found to be nil, and that in the vertical direction negligibly small. Stream angularity was shown by the usual procedure of inverting a wing model to be zero within the accuracy of measurement.

RESULTS

Range of Tests

Each model was tested at nominal angles of attack ranging by increments of 2° from -2° to 8°. Measurements of lift, drag, and pitching moment, together with base-pressure readings and other supplementary observations, were made at five values of tunnel total pressure. These pressures and the corresponding values of Reynolds number for wings and bodies are as follows:

Tunnel total pressure (lb/sq in)	Reynolds number for bodies (millions)	Reynolds number for wings (millions)
3	0.55	0.12
6	1.1	.24
12	2.1	.45
18	3.1	.66
25	4.2	.90

Selected schlieren photographs were also taken.

Data for the wings and combinations at high angles of attack and at the larger Reynolds numbers were limited by fouling of the model or sting against the shroud. All the results presented are free of fouling.

Most of the moment data were found to be useless because of excessive zero shifts, and were discarded. After this defect was remedied, moment readings were erroneous above only moderate values of lift because the balance beam brushed against an electrical lead. Only the moment readings were invalidated, the disturbance to the lift and drag being negligible. Because of these difficulties, the reliable pitching-moment results are fragmentary.

Schlieren Photographs

The character of the flow about the models is illustrated by typical schlieren pictures in figure 7. The upper photograph shows the bulbous body at zero angle of attack, while in the lower photograph the straight wing has been added. Both pictures were taken at a tunnel pressure of 18 pounds per square inch with an exposure time of a few microseconds. The knife edge of the schlieren apparatus was perpendicular to the flow direction and oriented so that regions of increasing density in the streamwise direction appear dark.

In the upper picture the principal shock waves caused by the model are, from left to right, the bow wave, a compression shock from the neck of the body, and the trailing shock behind the base, followed by a strong shock wave from the conical head of the balance housing. The intersection of each of these shock waves with the boundary layer on the glass side wall appears as a wavy hyperbolic line. The wake is seen to converge

behind the base of the body and flow turbulently along the shroud and balance housing. In the lower picture two additional shock waves spring from the leading and trailing edges of the wing.

The two shock waves cutting across those from the model are known to originate from a slight imperfection in machining the top and bottom walls of the tunnel. They fall downstream of all models and are known to be weak, so that they should not affect the results. The mottled appearance of the background is believed to result from turbulence of the boundary layer on the glass windows.

Aerodynamic Force Data

All force measurements are presented in the form of lift, drag, and pitching-moment coefficients. To obtain these results balance readings were multiplied by previously determined calibration constants to give the forces parallel and perpendicular to the balance beam and the pitching moment acting about the arbitrary reference axis. From these values and from the angle and position of the model relative to the beam, the lift, drag, and pitching moment of the model itself were calculated. These quantities were converted to coefficient form through division by appropriate reference dimensions and by the dynamic pressure calculated from

$$q = \frac{\gamma}{2} M^2 \left(1 + \frac{\gamma - 1}{2} M^2\right)^{-\frac{\gamma}{\gamma - 1}} H \qquad (1)$$

where

q dynamic pressure at the model

γ adiabatic exponent for air, taken to be 1.40

M Mach number at the model

H total pressure at the model

The proper value of H is slightly less than the value H' measured upstream in the low-speed section of the tunnel. The ratio H/H' has been determined experimentally as a function of specific humidity. Its value during this investigation (i.e., for specific humidity below 0.0008) lay always between 0.99 and 1.00, and was taken to be unity.

Coefficients for the bodies alone are referred here to the frontal area, and moments are taken about the base with the body length as reference. Coefficients for the wings and wing-body combinations are referred to the wing plan form area, moments being taken about the centroid of the plan form with the mean geometric chord as reference length. Thus in combinations involving the divided straight wing the reference area is entirely outside the body, while in every other case the reference area extends through the body. In this way coefficients for all the wings and combinations are referred to a common area, which permits direct quantitative comparison of the results. Values of Reynolds number are based upon the total length for bodies and upon the mean geometric chord of the plan form for wings.

Values given for total drag of bodies and combinations do

not necessarily apply to the models in free flight. No attempt was made to correct drags for the unknown effects of support interference. Independent tests indicate that these effects are a complicated function of the size and position of the model relative to the support, the shape of the model, and the Reynolds number. The effects are, however, confined mostly to the rearward portion of a model and are felt principally as a change in base pressure.

For this reason, and because base pressures cannot be predicted by theory, data are also presented for the total measured drags minus the base drags. The result is termed the "fore" drag. Base drags were calculated by multiplying the base area by the difference between free-stream static pressure and measured base pressure. Other investigations (reference 1) have shown that the pressure is constant over the base. Values of fore drag are believed to be relatively unaffected by support interference, and can be compared directly with theory.

Because all the stings were shrouded, no tare forces exist except for those on the small conical fitting used to support the wings. In an attempt to determine the magnitude of these forces, an equivalent dummy fitting was tested alone. The results which are shown in figure 8 for the highest value of Reynolds number are representative of those at other values. The coefficients are referred to the dimensions of the wings, and pitching moments are taken about the reference axis for the straight wing. Lift and moment were seen to be negligible compared with the lifts and moments experienced

by the wings and combinations. Drag is appreciable, however, and was accordingly subtracted as an aerodynamic tare from the measured drags of the wings plus the fitting.

Precision

The accuracy of the results can be estimated by considering in turn the uncertainty involved in determining angle of attack, in computing dynamic pressure, and in measuring forces with the strain-gage balance.

Zero angle of attack for each model was measured under static conditions by means of a dial indicator and a carefully leveled surface plate inside the test section, and is accurate to within $\pm 0.05^\circ$. Other angles were obtained by cranking the balance angle-of-attack mechanism always in the same sense to eliminate backlash and reading a counter to the nearest 0.01°; hence no additional error was introduced. Finally, all angles of attack were corrected for deflection of the support system under aerodynamic load. The deflections were calculated from the measured values of lift using elastic constants previously determined for the system by loading each model statically at its center of pressure. The calculated deflections agreed well with those observed directly with a telescope during the tests and should not be in error by more than $\pm 0.05^\circ$ even at the highest lift. Accordingly, the over-all uncertainty in angle of attack is believed to be never greater than $\pm 0.1^\circ$.

Calculated values of dynamic pressure are subject to

no flow inclination?

three known sources of error. First is the uncertainty in total-pressure readings, which are believed to be accurate to within ±1 millimeter of mercury. The corresponding uncertainty in dynamic pressure amounts to less than 1 percent at the lowest tunnel pressure, and falls to less than one-tenth of 1 percent at the highest pressure. Second, no correction was applied for the decrease in total pressure along the tunnel from the point of measurement to the model position, which the tunnel calibration showed to result from condensation of water vapor. Values of dynamic pressure may, on this account, be low by as much as 0.9 percent. Finally, equation (1) relating total pressure and dynamic pressure involves a knowledge of the test Mach number. The expression, however, is near a maximum with respect to M at the present value of approximately 1.53, and is consequently insensitive to small errors in the determination of Mach number.

Repeated calibration of the strain-gage balance during the course of the investigation showed fluctuations in the calibration constants of less than one-half of 1 percent over a period of several months. Calibration constants were found to be entirely unaffected by the extremes of pressure and temperature to which the interior of the balance is subjected in the course of a run. The zero readings, on the other hand, shifted over a wide range with changes in temperature. The variations could, however, be correlated with readings of thermocouples at the strain gages. The remaining

uncertainty in zero readings introduces small errors at the low values of Reynolds number, where the tunnel pressure and hence the forces on the models are small. At higher Reynolds numbers, however, which involve high tunnel pressures and large forces, the uncertainty in zero readings is usually unimportant.

At high values of lift, a further correction to the drag was necessary because lift and drag are not completely independent. The strain-gage springs deflect under load, the balance beam rotates slightly, and a small component of the lift acts upon the drag gage. Although small, this correction repeats poorly, introducing a maximum uncertainty of less than ± 0.002 into the drag coefficients of any model.

All coefficients are presented as if the test Mach number were constant. Actually its value fluctuated with tunnel pressure and humidity between the limits previously given, and the aerodynamic coefficients varied accordingly. To a first approximation, coefficients for wings are theoretically proportional to $(M^2 - 1)^{-\frac{1}{2}}$, and hence deviate from the mean by as much as ± 1 percent. Coefficients for bodies of revolution are according to linear theory much less responsive to slight variations in test Mach number.

The following table lists the total uncertainty introduced into each coefficient by errors in determining dynamic pressure, by errors in measuring forces with the balance, and by fluctuation of test Mach number. Values are listed for the

lowest and highest values of Reynolds number and vary linearly between these extremes.

Coefficient	Uncertainty at lowest Reynolds number	Uncertainty at highest Reynolds number
Body of revolution		
lift	±0.1	±0.03
drag	±.03	±.01
pitching moment	±.2	±.03
Wing or combination		
lift	±.02	±.01
drag	±.006	±.004
pitching moment	±.08	±.02

Inspection of the data indicates that experimental scatter lies generally within these limits.

The possible existence of nonrepeating errors resulting from unknown or uncontrollable causes, such as balance friction, was investigated by making repeated tests of several models. The basic body was tested twice, and the straight wing was tested at the start, the middle, and the end of the investigation. It is gratifying to see that all discrepancies between repeated runs lie within the limits of uncertainty prescribed above. Thus it is concluded that no appreciable source of error remains unaccounted for.

DISCUSSION

The results for wings and bodies alone will first be analyzed in detail in comparison with existing theory. This is done not only to establish a firm basis for the subsequent

discussion of wing-body combinations, but also because data for these elementary aerodynamic shapes are of interest in themselves, particularly insofar as they clarify the effects of scale at supersonic speeds. Following this analysis of the separate wings and bodies the main objective of the investigation - an evaluation of wing-body interaction - will be discussed.

Bodies

Comparable theory.- Experimental results for the three bodies of revolution can be compared with values predicted by the theoretical solutions of von Kármán and Moore for wave drag (reference 2) and of Tsien for lift and pitching moment (reference 3). These are linearized solutions which yield only first approximations to the actual aerodynamic characteristics. Both methods involve a stepwise solution which was carried out for the basic and bulbous bodies using 14 and 18 integration stations, respectively. The methods are not applicable to the blunt body. The actual computing procedure employed was that of reference 4. The resulting pressure distributions are presented as a matter of interest in figure 9. For the bulbous body the pressure distribution at zero angle of attack was calculated over the head only, because pressures along the cylindrical shank exert no net force. The pressure on the conical nose given by the mathematically exact theory of Taylor and Maccoll (reference 5) is also shown to indicate the

degree of approximation involved in the linear theory.

Lift.- Figure 10 presents the lift characteristics of the three bodies of revolution. Lift coefficient is plotted versus angle of attack at five values of Reynolds number. For comparison the theoretical variation is also shown by a dashed line for the basic and bulbous bodies.

The bodies, being axially symmetrical, should of course show vanishing lift at zero angle of attack. Their consistent failure to do so can be attributed only to errors in force measurement, probably a result of the remaining uncertainty in balance zero shift with temperature. In general, the discrepancy lies inside the limits of error listed previously.

For all three bodies, lift coefficient increases at first linearly with angle of attack, as the simple theory indicates; only above 6° angle of attack do the experimental values of lift begin to rise more rapidly. Analogy to the case of airfoils suggests that such an upward curvature might be predicted by a theory more refined than the first-order treatment employed. However, the departure from linearity is here so abrupt that it is more likely the result of another cause, perhaps flow separation. Tsien notes (reference 3) that in the event of separation the lift will increase at greater than a linear rate.

Experimental values of lift-curve slope depend upon Reynolds number, as shown in figure 11. For each body lift-curve slope is seen to fall initially with increasing

Reynolds number, remaining nearly constant beyond about three millions. This constant value is, for the basic body, equal to that predicted by theory. Blunting the nose increases the slope at high Reynolds numbers. For the bulbous body the final constant value of lift-curve slope is considerably less than theory, and is about equal to that for the basic shape. The reason for this may be in part that the effective shape of the bulbous body approaches that of the basic body. Schlieren observation indicates that the flow departs from the surface of the bulbous body just beyond the point of maximum thickness, probably as a result of laminar separation. In figure 7(a) this effect is evident from the thin dark line on the top of the body. It cannot be observed on the bottom, probably because of insufficient optical sensitivity; but the attendant "catwhisker" shock wave, which marks its beginning, is clearly evident. The separation apparently starts slightly ahead of the theoretical adverse pressure gradient shown in figure 9.

Drag.- In figure 12 the total-drag and fore-drag coefficients of each body are plotted versus angle of attack. Theoretical values are also shown for the basic and bulbous bodies. No theory is shown for the blunt body since the method is inapplicable.

Consider first the general effects of scale upon drag. It is seen that total-drag coefficients of all three bodies exhibit large variations with Reynolds number. Comparison with the corresponding fore-drag coefficients makes it evident

that this is the result largely of scale effect upon base pressure. However, considerable scale effect upon fore drag remains. The remaining effect is much too great to be attributed to changes in skin friction, if incompressible values of skin-friction coefficient are assumed. This assumption appears to be justified by the results of references 6 and 7.

In the case of the bulbous body, the variation of fore drag with Reynolds number can probably be ascribed to the flow separation which was seen to occur near the point of maximum thickness. Independent tests suggest that the extent of separation varies markedly with scale, although schlieren photographs, which might confirm this for the bulbous body, are not available throughout the range of Reynolds number. Consideration of the theoretical pressure distribution indicates that the experimental variation of fore drag is less than the change which would result if the flow separated tangentially at the point of maximum thickness. Only partial progression with Reynolds number between separated and unseparated flow is thus sufficient to account quantitatively for the observed change in fore drag.

No separation was observed which might account for the effects of scale upon the fore drags of the other two bodies. It is likely, however, that variation of pressure at the rear of a body is not confined solely to the flat base, but is

transmitted some distance upstream through the boundary layer. The basic and blunt bodies are boat-tailed, so that such a variation would exert a resultant force in the drag direction. The magnitude of this force has been estimated on the assumption that the base pressure acts undiminished over the entire boat-tail and has been found to more than account for the observed changes in fore drag. No explanation is known for the fact that fore drag exhibits a much greater scale effect for the blunt body than for the basic body.

It is evident from figures 12(a) and 12(c) that the rate of increase of drag coefficient with angle of attack is underestimated by theory. The agreement improves as Reynolds number is increased, but even at the upper limit of the investigation the fore drags of the basic and bulbous bodies increase several times faster than the theoretical prediction.

Consider now the particular case of minimum drag. Figure 13 shows the effects of scale upon minimum drag coefficients of the three bodies. Both minimum fore drag and minimum total drag are seen to increase with Reynolds number. Nearly constant values are attained for the basic body at a Reynolds number of three millions, and apparently also for the bulbous body at the highest test value. Minimum drags of the blunt body continue to rise up to the limit of the investigation. Blunting the basic body increases both minimum fore drag and minimum total drag, except at the lowest Reynolds number. This one exception appears so unlikely that

it must be presumed to be due to experimental error, lying as it does just inside the limits of uncertainty listed previously.

Also shown for the basic and bulbous bodies in figure 13 are the theoretical values of fore drag, consisting of the theoretical wave drag plus the skin-friction drags for both laminar and turbulent flow. Values of skin-friction coefficients were assumed appropriate to incompressible flow. At low Reynolds numbers, minimum fore-drag coefficients are seen to fall below either theory. As discussed previously, this discrepancy results from separation in the case of the bulbous body, and from high base pressures acting through the thick boundary layer to increase the pressures over the boat-tail in the case of the basic body. At higher Reynolds numbers, however, experimental values of minimum fore drag lie between the narrow limits of theory modified for laminar and turbulent skin friction. In view of the approximate nature of the theory, such close agreement is perhaps fortuitous.

Pitching moment.- Reliable moment data were obtained only for the basic body. These are presented in figure 14 together with the prediction of linear theory. It is seen that a zero shift (which lies inside the suggested limits of uncertainty) has caused a serious displacement of the moment curve at the lowest Reynolds number. Otherwise the data appear gratifyingly good. The increase of moment coefficient

with angle, like that of lift, departs from linearity above 6°. The slope of the moment curve agrees well with theory throughout the range of Reynolds numbers investigated, and is not subject to scale effect.

Wings

Comparable theory.- Experimental results can, in the case of the straight wing, be compared with values predicted by theory if the effect of taper is neglected. In the case of the sweptback wing, on the other hand, it will be seen that existing theory is not applicable.

The aerodynamic characteristics of the straight wing are, except for the effects of taper and finite span, predicted by two-dimensional supersonic airfoil theory. Here the solution was obtained by the method of successive oblique shock waves and isentropic expansions, which is presented in convenient form in reference 8. For the particular airfoil section employed this "shock-expansion" method represents, in fact, the exact inviscid solution for conditions on the airfoil surface. The theory fails if the flow changes to subsonic behind the oblique shock wave at the leading edge, but the angle of attack at which this occurs was not attained in the present investigation.

The effects of taper cannot be accounted for theoretically, but are probably very small. The effects of finite span can, however, be accounted for approximately. Linear theory

indicates that at supersonic speeds the effects are confined solely to the triangular portions of the wing intercepted by the Mach cones springing from the front of each wing tip. Busemann has investigated the case of a rectangular flat plate (reference 9) and found that to first order the lift within the tip regions is half what it would be in the absence of any effect. This result for the rectangular flat plate was assumed to apply approximately to the present tapered wing of 5-percent-thick section. The theoretical section characteristics were modified accordingly. That is, the section coefficients were modified by the factors which would apply to an equivalent rectangular flat plate. The equivalent rectangular plan form was chosen so that the Mach cones springing from the wing tips intercept the same percentage of total area as on the actual tapered plan form. This procedure yields what is believed to be the best prediction obtainable from existing theory. It is this theory that will be employed in the discussion unless otherwise noted.

For the sweptback wing no such refined theoretical treatment has been developed. The first-order theory for a constant-chord sweptback wing of infinite span (reference 10) applies in the present case for only a short distance behind the leading edge. Furthermore, in attempting to use the simple theory only within this region, it is found that the bow wave will always be detached from the present airfoil

section, and consequently the theory is never applicable. The reason for the detachment is that near the leading edge to a first approximation only the normal component of velocity is effective, and the corresponding Mach number is less than 1.16. Then the bow wave will theoretically detach whenever the angle through which the flow is compressed at the leading edge exceeds 2.8°. Since the leading-edge angle of the sweptback wing is greater than twice this value, detachment will always occur. Detachment was observed experimentally with the schlieren apparatus for an angle of compression at the leading edge of only 3°. In view of these objections, no comparison with theory is made in the case of the sweptback wing.

Lift.- Lift characteristics of the straight and sweptback wings are presented in figure 15. Variation of lift coefficient with angle of attack is shown, together with theory in the case of the straight wing.

On the whole, lift results are qualitatively similar to what would be anticipated from theory. Lift coefficient increases at first almost linearly with angle of attack, and slightly more rapidly at high angles. Angle of zero lift varies only slightly with Reynolds number for both wings, as shown in figure 16. Its value in the case of the straight wings exceeds by $\frac{1}{2}$° that predicted from theory. The same shift was observed by Ferri for a two-dimensional airfoil of similar section tested at comparable values of Mach and Reynolds

number (reference 11). Ferri obtained pressure-distribution measurements on other profiles which indicate that the shift can be attributed to flow separation on the low-pressure surface near the trailing edge.

Figure 16 shows that experimental values of lift-curve slope depend upon Reynolds number for both wings. Slopes are seen to increase with Reynolds number up to one-half million, probably as a result of rearward movement of the separation point. Beyond this value of Reynolds number, lift-curve slopes of both wings are independent of scale up to the limit of the investigation. For the straight wing, the constant value, though less than the theoretical section value, is almost 4 percent greater than the theoretical value for finite span. This discrepancy can probably be attributed to the influence of the fitting which supports the wing. It will be shown later when discussing wing-body interaction that, at supersonic speeds, lifting pressures carry over from a wing onto a body for some distance downstream from the trailing edge. The projected area of the support fitting is 7 percent of the wing area, so that only a partial carry-over of lift would account for the 4-percent excess.

Angular deflection of the wings under aerodynamic load is a complicating factor. In the case of the straight wing it causes no difficulty since the wing merely becomes slightly bowed, with every spanwise section remaining at the same angle of attack. The sweptback wing, on the other hand,

twists under load so that the angle of attack decreases progressively along the span. In the present investigation, measurements showed that the decrease amounted to as much as 1° at the tips of the sweptback wing. For this reason the actual angle of attack of the whole wing might be considered indeterminate, so that the true characteristics of the wing would be obscured by twist. From another point of view, however, the angular deflection is more apparent than real. The argument depends upon the simple theory of sweepback (reference 10) which, despite the objections previously advanced, may perhaps apply to the present wing in a general way. Consider how a sweptback wing deflects elastically under load. It is apparent that the angle of attack of streamwise sections will decrease from the root to the tip. The angle of attack measured normal to the leading edge will remain, however, nearly constant along the span. It is this latter angle which, according to simple sweep-back theory, determines the aerodynamic characteristics. Thus, according to this theory, the characteristics of the sweptback wing will not be affected by twist. That this latter reasoning may be the more nearly correct is borne out by figure 16 which shows the effect of scale upon the lift-curve slope of the sweptback wing. From a Reynolds number of one-half million up to the limit of the investigation the wing loading, and hence the angle of tip deflection, increases several fold. Lift-curve slope, however, remains unchanged.

Drag.- Drag characteristics of the straight and sweptback wings are presented in figure 17. Theoretical wave drag is also shown for the straight wing.

For both wings, drag coefficients are independent of Reynolds number above one-half million. Thus in figures 17(a) and 17(b) the test points for the three highest values of Reynolds number define a single curve. In order to make this clearer in the case of the straight wing, these points have been replotted separately from those for the two lower Reynolds numbers, as shown in the upper half of figure 17(a). Below one-half-million Reynolds number, the drag falls progressively as the scale increases, probably as a result of the decrease in skin friction which accompanies increasing Reynolds number. This decrease apparently more than offsets the rise in pressure drag which would be expected to result from the rearward movement of the separation point previously indicated in the discussion of lift-curve slope.

Scale effect upon minimum drag is typical qualitatively of that at any angle of attack. Figure 18 shows the variation of minimum drag coefficient with Reynolds number for both wings. Also shown for the straight wing are the theoretical values of drag obtained by adding low-speed values of laminar and turbulent skin friction to the theoretical wave drag. The agreement between experiment and the theory including laminar friction is remarkable. On the other hand, agreement with the theory including turbulent friction is poor. Thus it seems likely that within the Reynolds number range of these tests

the boundary layer is predominantly laminar over at least the straight wing.

At higher angles of attack, figure 17(a) shows that the agreement is less perfect between theoretical and experimental values of drag for the straight wing. Beyond about 5° the measured drag at the higher Reynolds numbers is lower than the theoretical wave drag, even when skin friction is neglected. This behavior is in accord with Ferri's findings for an airfoil of similar section. (See reference 11.)

It has been seen that both the lift and drag characteristics of the two wings are independent of scale above one-half million Reynolds number. Consequently the curves of figure 19 showing drag coefficient as a function of lift coefficient likewise exhibit no scale effect beyond this value.

Curves of drag coefficient and lift-drag ratio as a function of lift coefficient are compared for the straight and sweptback wings in figure 20 for the range of Reynolds numbers in which scale effect is absent. The sweptback wing is seen to be superior to the straight wing in that it displays approximately 10 percent lower drag and correspondingly higher lift-drag ratio at any value of lift coefficient throughout the range investigated. It must be emphasized that this comparison is presented simply as a matter of interest. It was not the purpose of this investigation to compare the relative merits of swept and unswept plan forms. Consequently no attempt was made in designing the models to choose an optimum amount of sweepback; very probably some other angle would have proved more

favorable. In any event, it is not to be expected that the selection of the best sweepback angle for a given Mach number can be divorced from the choice of airfoil section.

Pitching moment.- Pitching-moment measurements for the wings were severely restricted by the balance defect mentioned previously and, being small, are likewise subject to considerable experimental scatter. The limited reliable data are presented in figure 21 for the straight and sweptback wings.

Within the limits of experimental uncertainty, moment coefficients for the straight wing appear to agree with theory. The slope of moment versus angle of attack is, however, definitely at variance with the theoretical prediction, having, in fact, the opposite sign. As in the case of lift-curve slope, the disagreement probably results from the influence of the fitting, which supports the wing. Lift carried over onto the fitting, which projects behind the trailing edge, would tend to make the observed slope of the moment curve negative, as it is in figure 21(a). It was not considered feasible, however, to attempt to correct the results for this disturbance.

Figure 21(b) shows that the pitching-moment coefficients for the sweptback wing, referred to the centroid of the plan form, are similar to those for the straight wing. The slope of the moment curve is, however, slightly less negative. The fitting probably exerts a smaller influence in this case

because it is closer to the moment axis. Hence the true values of moment coefficient may be virtually identical for the straight and sweptback wings at all angles of attack. In any event the values are small, so that the center of pressure lies nearly at the center of area for both wings. No scale effect upon the pitching-moment characteristics of either wing can be discerned.

Wing-Body Combinations and Interaction

The aerodynamic characteristics of the eight wing-body combinations are of interest chiefly in determining the effects of interaction. Accordingly, the lift and drag of the combinations will not be discussed separately but only in comparison with the characteristics of the separate components.

Lift interaction.- When the investigation was undertaken it was anticipated that the portion of wing area blanketed by a body might prove only partially effective in the production of lift. The extent of its effectiveness was, of course, to be evaluated by comparing the sum of the lifts of the separate wings and bodies with the lift of each resultant combination.

This comparison is made in figure 22. Variation of lift coefficient with angle of attack is shown by a solid line for each combination of a wing plan form through a body. In cases where the plan form was also tested outside the body (using the divided wing), the result is shown on the same graph by a broken line. For comparison, a dashed line shows

the sum obtained by adding the measured lifts of the separate wing and body. All coefficients have been referred to a common reference area, that of the wing plan forms.

It is at once evident that the lift-curve slope for a combination comprising a plan form mounted through a body is practically identical in every case with the sum of the slopes for the component wing and body. This observation applies to either the straight or sweptback plan form together with any one of the three different bodies. Furthermore, it is valid throughout the entire range of Reynolds numbers investigated. The accuracy of this result is emphasized by the data shown in figures 22(a) and 22(c) for the combination of the plan form mounted outside (rather than through) the body. The lift-curve slope of this alternative combination is much greater than the total for its components. Thus at 1.53 Mach number the effect of interaction is such that in estimating the lift of a combination from the characteristics of its components, the portion of wing area blanketed by the body should be considered completely effective.

The mechanism by which lift is carried over across the body would be clarified by pressure-distribution measurements. Certain German results have recently become available which to some extent explain this matter. Reference 12 presents measurements through a broad speed range of the lift distributions over a simple body of revolution and a missile

comprising nearly the same body plus a wing. Consideration of the distribution of normal force shows that the result of adding a wing is distinctly different at subsonic and supersonic speeds. At subsonic speeds additional lift acts upon the portion of the body directly between the two halves of the wing. At supersonic speeds, however, additional lifting pressures act on the body for a considerable distance downstream of the wing. It appears reasonable to suggest that the lift carried over onto the body is shifted downstream roughly within an area defined by the Mach cones springing from the leading and trailing edges of the wing root. Thus the conclusion reached in the present investigation - that the blanketed portion of wing is completely effective in producing lift - is probably correct only when the wing is located well ahead of the base of the body. Otherwise considerable lift may be lost. In the case of a tail surface, for example, the lifting pressures which would otherwise act downstream will disappear. The portion of the lifting surface blanketed by the body will then be only partially effective in producing lift.

Mention must be made of another probable restriction. Consideration of the limiting case of vanishingly small wing span makes it obvious that the rule becomes invalid when the wing span is short compared with the body diameter. The exact limit cannot, of course, be determined from the results of this investigation. It is likely that the rule will apply for ratios of wing span to body diameter considerably smaller than

those employed here.

Experimental angles of zero lift for the combinations are several tenths of a degree less than those obtained from the component results, except when the bulbous body is involved. It was previously noted that the experimental zero-lift angle for the straight wing alone exceeds theory by approximately the same amount, and the difference was attributed to separation. This suggests that the presence of the body inhibits flow separation over the wing, except when the bulbous body is employed.

Drag interaction.- When a wing is mounted through a body, blanketing of the midsection of the wing will tend to reduce the drag of the combination because the exposed area is less. On the other hand, it is known that mutual interference of wing and body usually tends to increase the drag. Depending upon which of these effects predominates, the net drag of the combination will be either greater or less than the sum of the drags of its components.

A comparison is made in figure 23, in the same manner as in the case of lift, between the fore-drag coefficients of the various wing-body combinations and the sums of the drags of the separate wings and bodies. Fore drag is considered, rather than total drag, so that the comparison will not be complicated by the possible effects of support interference upon base pressure.

Inspection of figure 23 leads to the conclusion that, in general, the drag of the combination comprising the wing plan form mounted through the body is equal to the sum of the drags of its components. The accuracy of this conclusion is not so great as in the case of lift. The agreement is generally poor at the lowest values of Reynolds number. At higher Reynolds numbers a systematic variation with body shape is evident. For combinations involving the basic body (figs. 23(a) and 23(b)) the drag is ordinarily slightly greater than the sum for the separate wing and body. When the blunt body is involved (figs. 23(c) and 23(d)) the two values are essentially equal, while with the bulbous body (figs.23(e) and 23(f)) the drag of the combination is slightly smaller than the sum for its components. Figures 23(a) and 23(c) show, however, that the agreement is always much better than it is for the alternative combination of the plan form mounted entirely outside the body. Hence it appears that for all practical purposes the drag decrease effected by blanketing a portion of the wing is counterbalanced by the increase resulting from interaction.

The physical reason for this rule is not so apparent as in the case of lift, and no pressure-distribution measurements are available to clarify the mechanism involved. It is again evident, however, that the rule becomes invalid when the wing span is short in comparison with the body diameter. The rule may also fail when the lifting surface is near the rear of the

body, as with a tail plane.

While this comparison has been confined to fore drag, which is believed to be relatively free of support interference, exactly the same conclusions apply to total drag. This is demonstrated in figure 24 for only one typical case, the straight wing plan form mounted through the blunt body.

Moment interaction.- No reliable data were obtained relating to the effect of interaction upon pitching-moment characteristics. In discussing lift interaction, it was noted that for a combination the lift which is carried over from the wing onto the body is displaced downstream. The moment of a body is negligible compared with that of a wing, so that it seems likely that the center of pressure for a combination would lie behind that of the wing alone.

Applicability of Results

The conclusions deduced from this investigation regarding the aerodynamic characteristics of wings and bodies, the effects of scale, and the effects of interaction upon the lift and drag of combinations at supersonic speeds are strictly applicable only at Mach numbers close to the test value of 1.53. It is logical to assume, however, that these results apply at least approximately for other supersonic Mach numbers neither very large nor very close to unity. Further investigation is required to show to what extent changes in Mach number affect either the generality of the

conclusions or the restrictions to their applicability which have been suggested.

It is evident that even an approximate theoretical solution for supersonic flow over some simple combination of plane lifting surface and body of revolution would be welcomed by the practical aerodynamicist.

CONCLUSIONS

The following conclusions were deduced from tests at 1.53 Mach number of several supersonic wings, bodies of revolution, and resulting combinations:

1. Up to the highest Reynolds numbers reached in the investigation, aerodynamic characteristics of the straight and sweptback wings are independent of scale above a Reynolds number of one-half million. Beyond that value, the characteristics of the straight wing, except for angle of zero lift and drag at high angles of attack, are closely predicted by existing theory.

2. Aerodynamic characteristics of the two sharp-nose bodies of revolution appear to be nearly independent of scale between Reynolds numbers of three or four millions and the highest values reached in the test. Beyond those values, their characteristics, except for drag at high angles of attack, are predicted reasonably well by existing linear theory up to angles of attack of 6°. The blunt body continues to show scale effect up to the limit of this investigation.

3. In estimating lift and drag of a wing-body combination from the characteristics of its components, the portion of wing area blanketed by the body should be considered completely effective aerodynamically. This rule probably fails if the wing is close to the base of the body, or if the wing span is small compared with the body diameter.

Ames Aeronautical Laboratory,
National Advisory Committee for Aeronautics,
Moffett Field, Calif.

Milton D. Van Dyke

Milton D. Van Dyke,
Aeronautical Engineer.

Approved:

H. Julian Allen

H. Julian Allen,
Aeronautical Engineer.

REFERENCES

1. Ferri, Antonio: Supersonic-Tunnel Tests of Projectiles in Germany and Italy. NACA ACR No. L5H08, 1945.

2. von Kármán, Theodor, and Moore, Norton B.: Resistance of Slender Bodies Moving with Supersonic Velocities, with Special Reference to Projectiles. Trans. A.S.M.E., vol. 54, no. 23, Dec. 15, 1932, pp. 303-310.

3. Tsien, Hsue-Shen: Supersonic Flow over an Inclined Body of Revolution. Jour. Aero. Sci., vol. 5, no. 12, Oct. 1938, pp. 480-483.

4. Sauer, Robert: Theoretische Einführung in die Gasdynamik (Theoretical Introduction to Gas Dynamics). Springer-Verlag (Berlin), 1943, reprinted by Edwards Bros., Ann Arbor, Mich., 1945.

5. Taylor, G. I., and Maccoll, J. W.: The Air Pressure on a Cone Moving at High Speeds. Proc. Roy. Soc. (London), ser. A, vol. 139, no. 838, Feb. 1, 1933, pp.278-311.

6. Theodorsen, Theodore, and Regier, Arthur: Experiments on Drag of Revolving Disks, Cylinders and Streamline Rods at High Speeds. NACA ACR No. L4F16, 1944.

7. Keenan, Joseph H., and Neumann, Ernest P.: Friction in Pipes at Supersonic and Subsonic Velocities. NACA TN No. 963, 1945.

8. Ivey, H. Reese, Stickle, George W., and Schuettler, Alberta: Charts for Determining the Characteristics of Sharp-Nose Airfoils in Two-Dimensional Flow at Supersonic Speeds. NACA MR No. L6C01, 1946.

9. Busemann, Adolf: Infinitesimale kegliche Überschallströmung (Infinitesimal Conical Supersonic Flow). Jahrbuch 1942/43 der Deutschen Akademie der Luftfahrtforschung.

10. Busemann, A.: Aerodynamic Lift at Supersonic Speeds. Rep. No. 2844, Ae. Techl. 1201, British A.R.C. (Translation), Feb. 1937.

11. Ferri, Antonio: Experimental Results with Airfoils Tested in the High-Speed Tunnel at Guidonia. NACA TM No. 946, 1940.

12. Kurzweg: Die Aerodynamische Entwicklung der Flakrakete "Wasserfall" (The Aerodynamic Development of the Antiaircraft Rocket "Wasserfall"). Wasserbau-Versuchsanstalt Archiv Nr. 171 gK., March 1945.

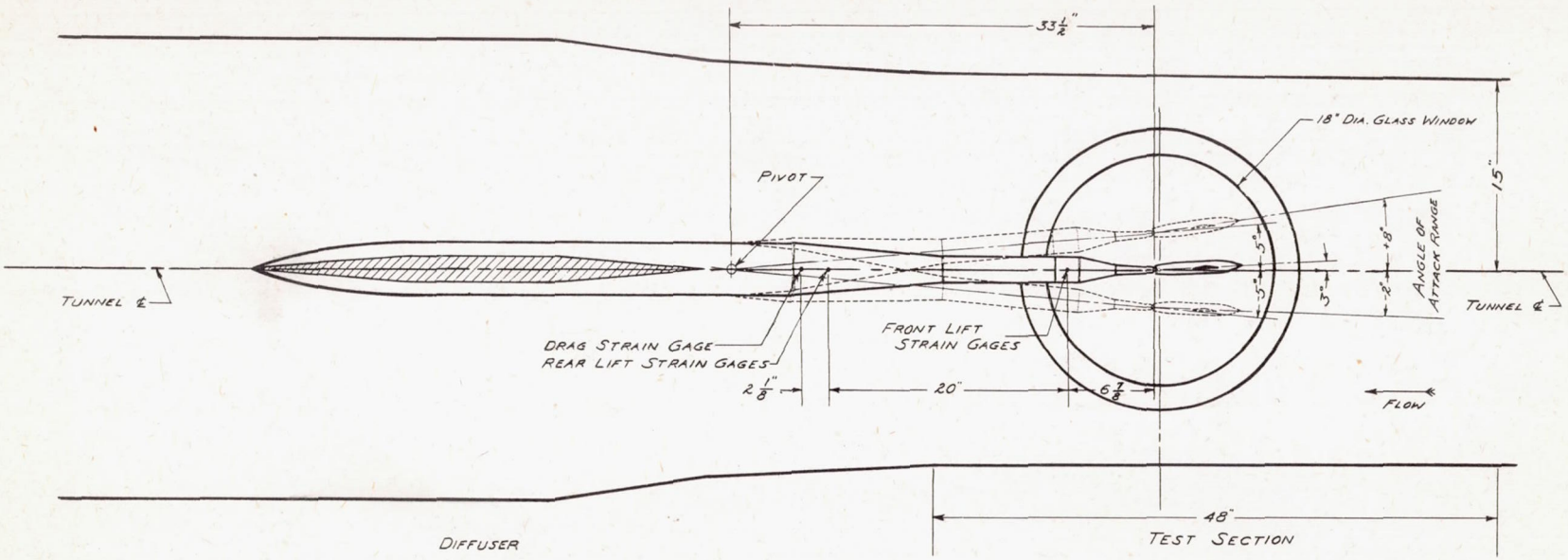

NATIONAL ADVISORY COMMITTEE FOR AERONAUTICS

FIGURE 1. - ELECTRIC STRAIN-GAGE BALANCE INSTALLED IN THE TUNNEL

CONFIDENTIAL

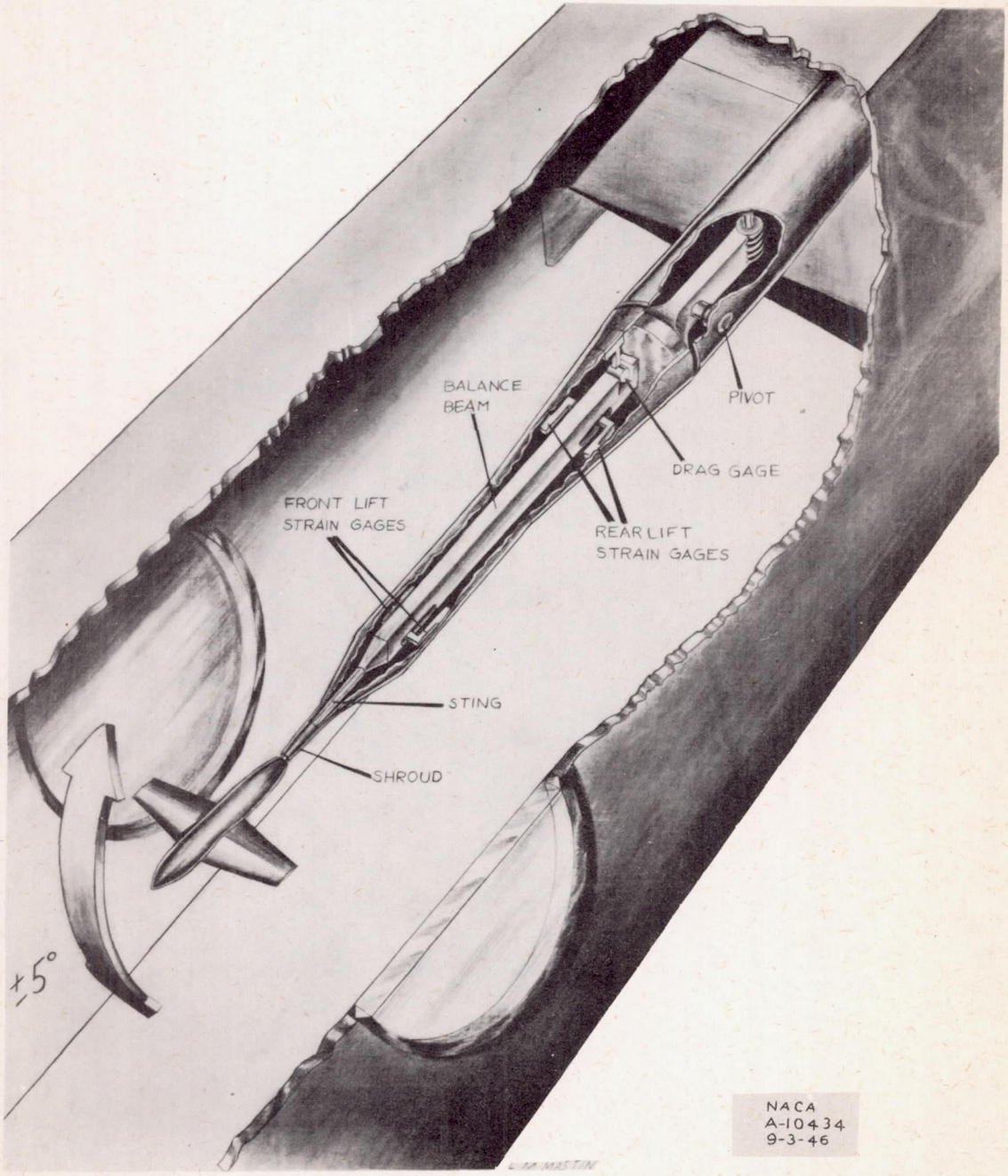

Figure 2.- Schematic diagram of the electric strain gage balance.

CONFIDENTIAL

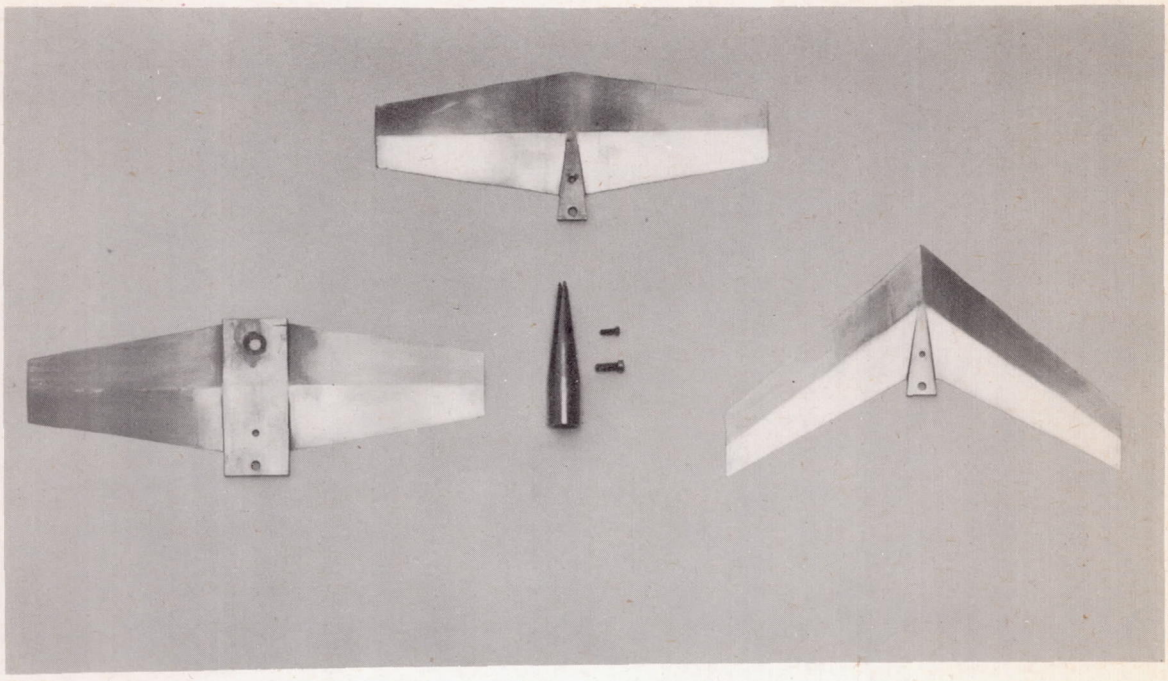

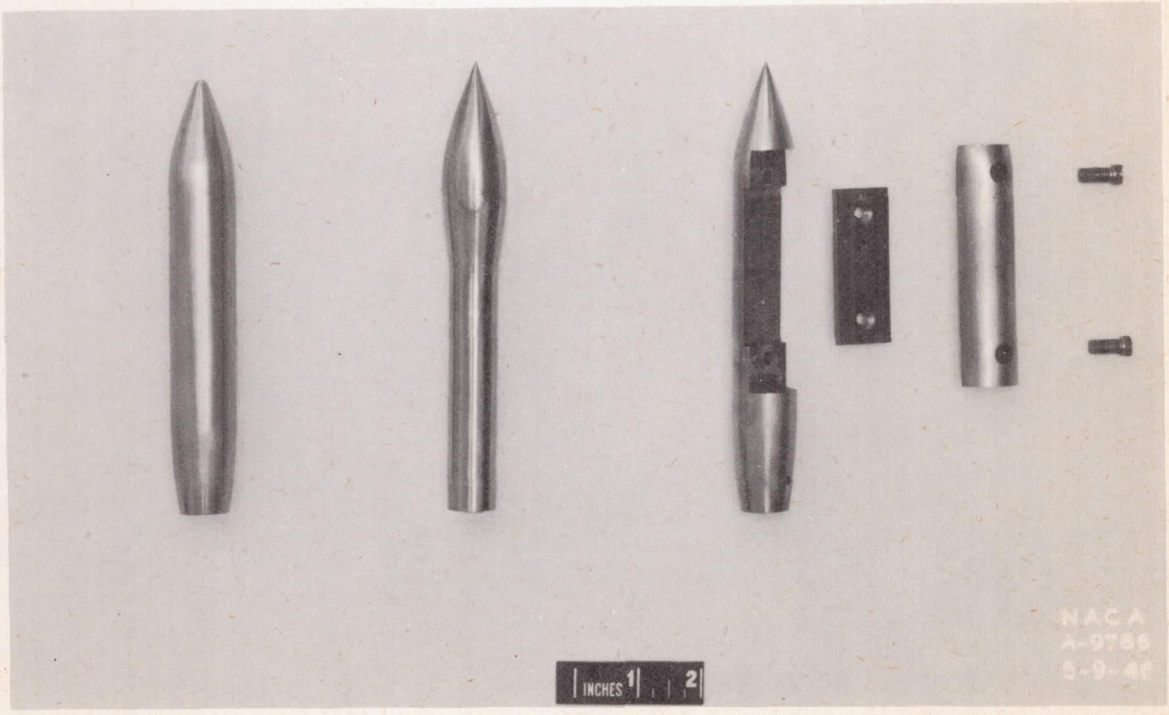

Figure 3.- Wing and body models tested.

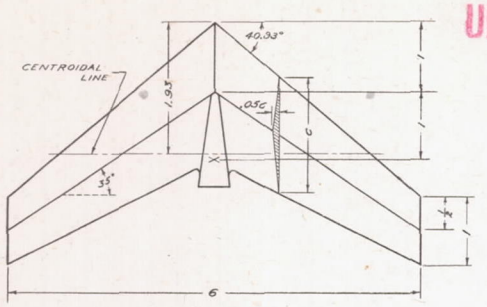

SWEPTBACK WING

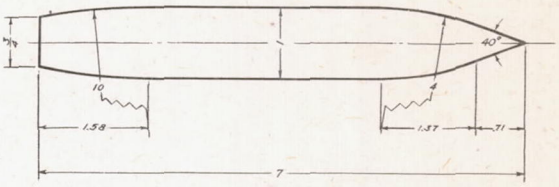

BASIC BODY

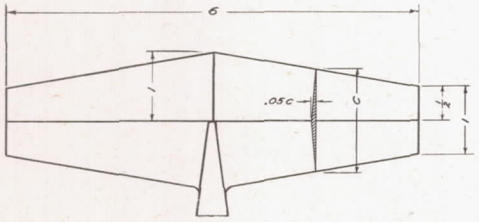

STRAIGHT WING

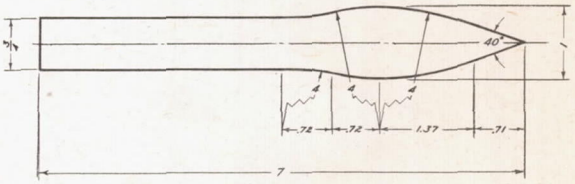

BULBOUS BODY

NOTE: ALL DIMENSIONS IN INCHES

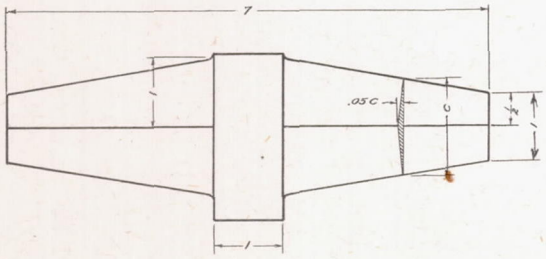

DIVIDED STRAIGHT WING

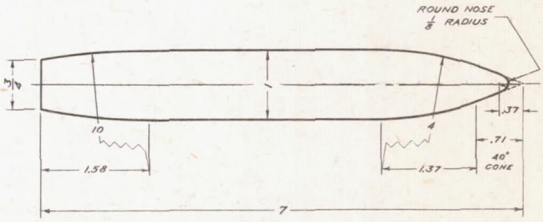

BLUNT BODY

NATIONAL ADVISORY COMMITTEE FOR AERONAUTICS

FIGURE 4 - DIMENSIONS OF MODELS

NOTE: ALL DIMENSIONS IN INCHES

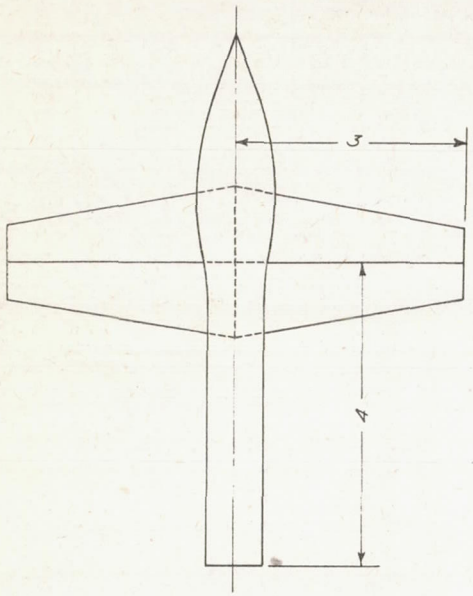

STRAIGHT WING PLANFORM
THROUGH BULBOUS BODY

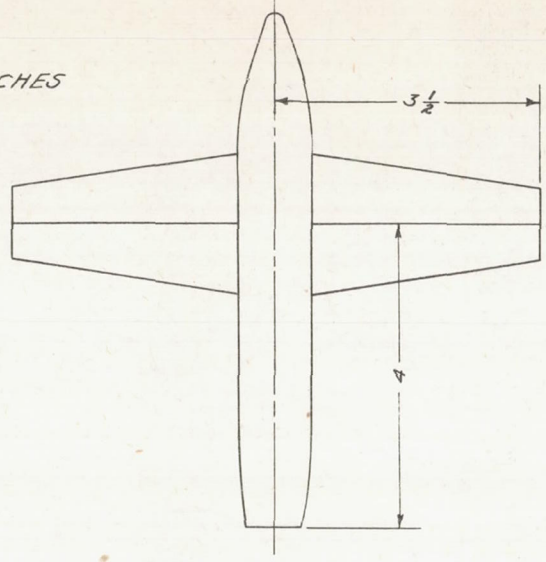

STRAIGHT WING PLANFORM
OUTSIDE BLUNT BODY

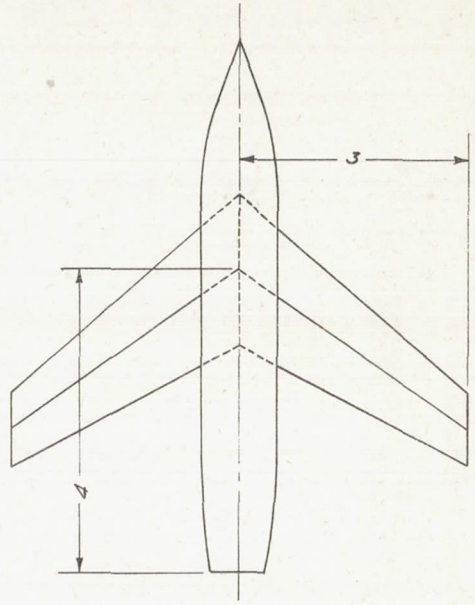

SWEPTBACK WING PLANFORM
THROUGH BASIC BODY

NATIONAL ADVISORY
COMMITTEE FOR AERONAUTICS

FIGURE 5 - TYPICAL WING-BODY COMBINATIONS

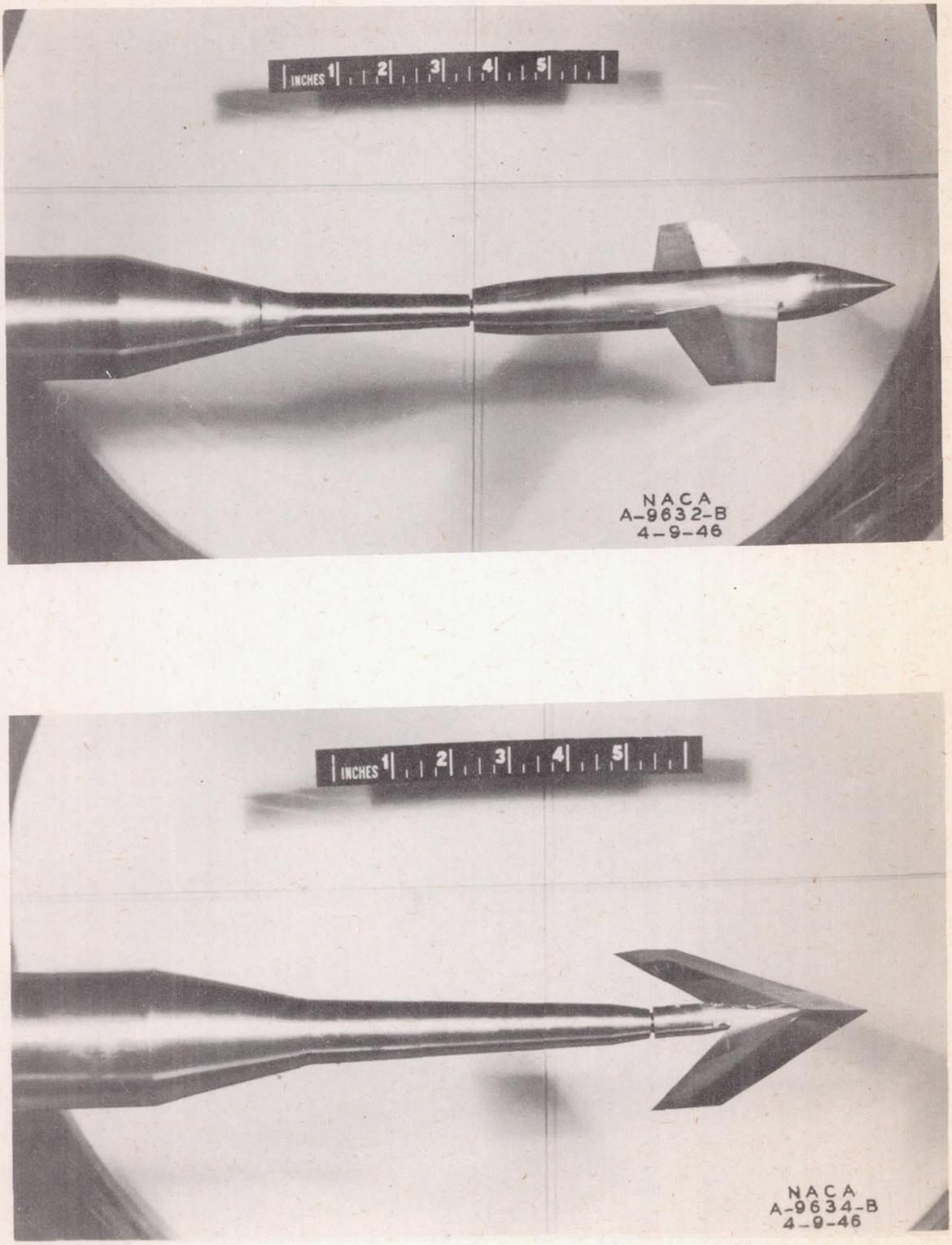

Figure 6.- Typical models mounted on strain-gage balance in test section of Ames 1- by 3-foot supersonic wind tunnel No. 1.

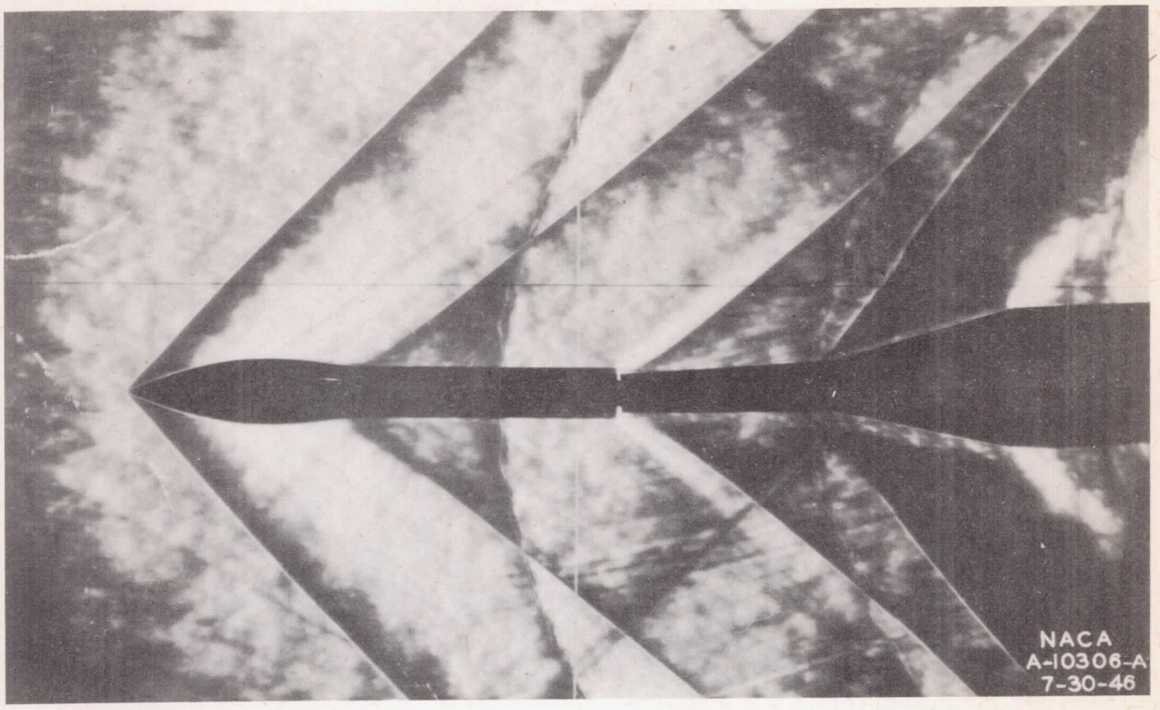

(a) Bulbous body, $\alpha = 0^{\circ}$.

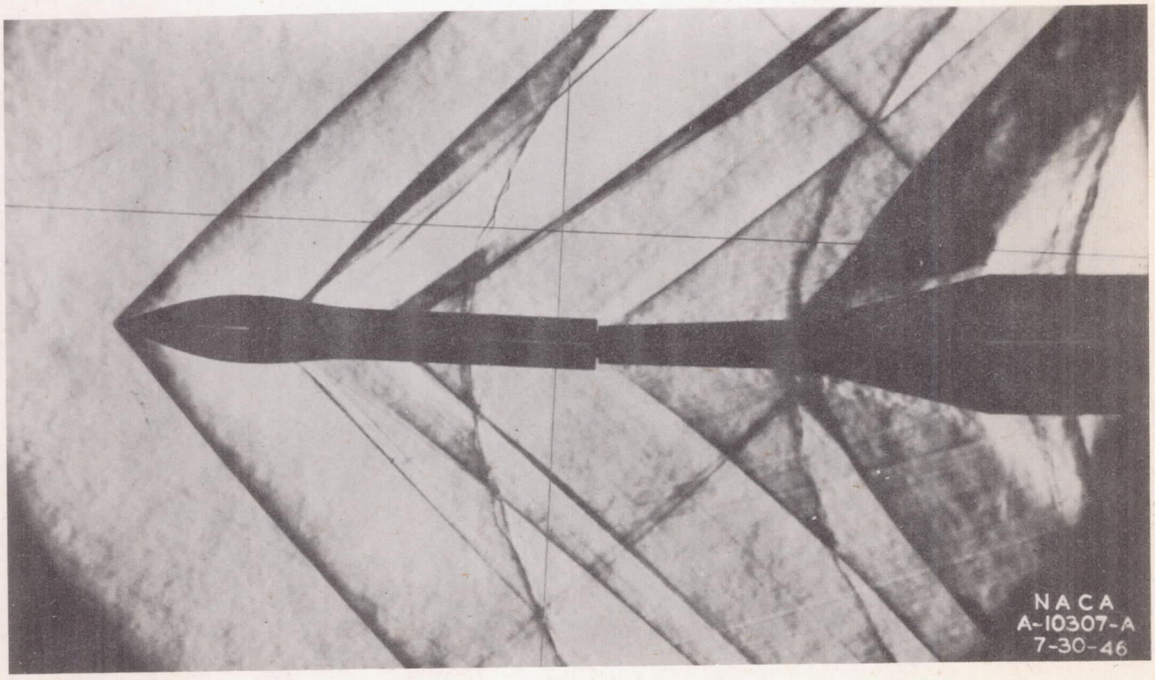

(b) Combination of bulbous body and straight wing, $\alpha = 0^{\circ}$.

Figure 7.- Typical schlieren photographs at a tunnel pressure of 18 pounds per square inch.

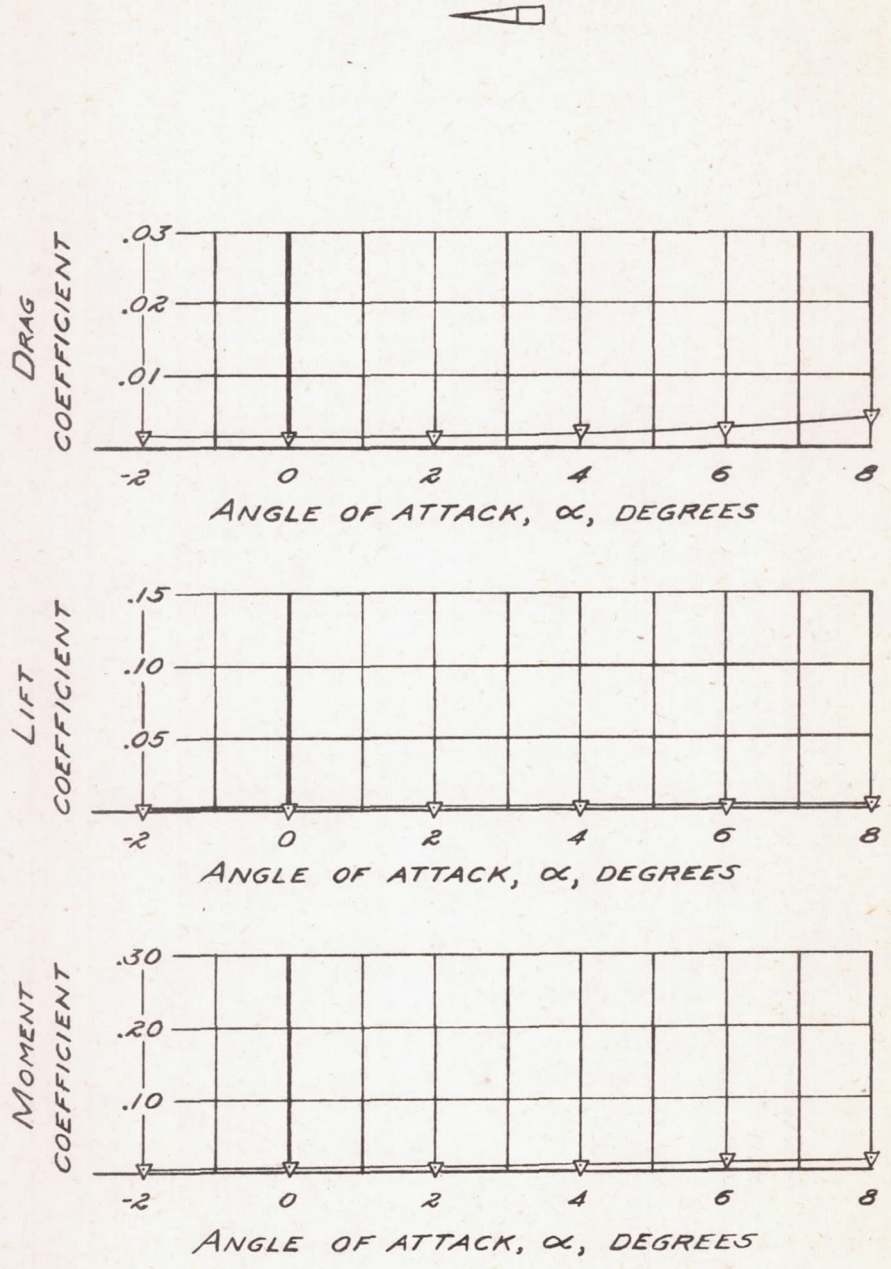

NATIONAL ADVISORY
COMMITTEE FOR AERONAUTICS

FIGURE 8. - VARIATION OF DRAG, LIFT, AND PITCHING-MOMENT COEFFICIENTS WITH ANGLE OF ATTACK AT HIGHEST REYNOLDS NUMBER FOR DUMMY WING FITTING.

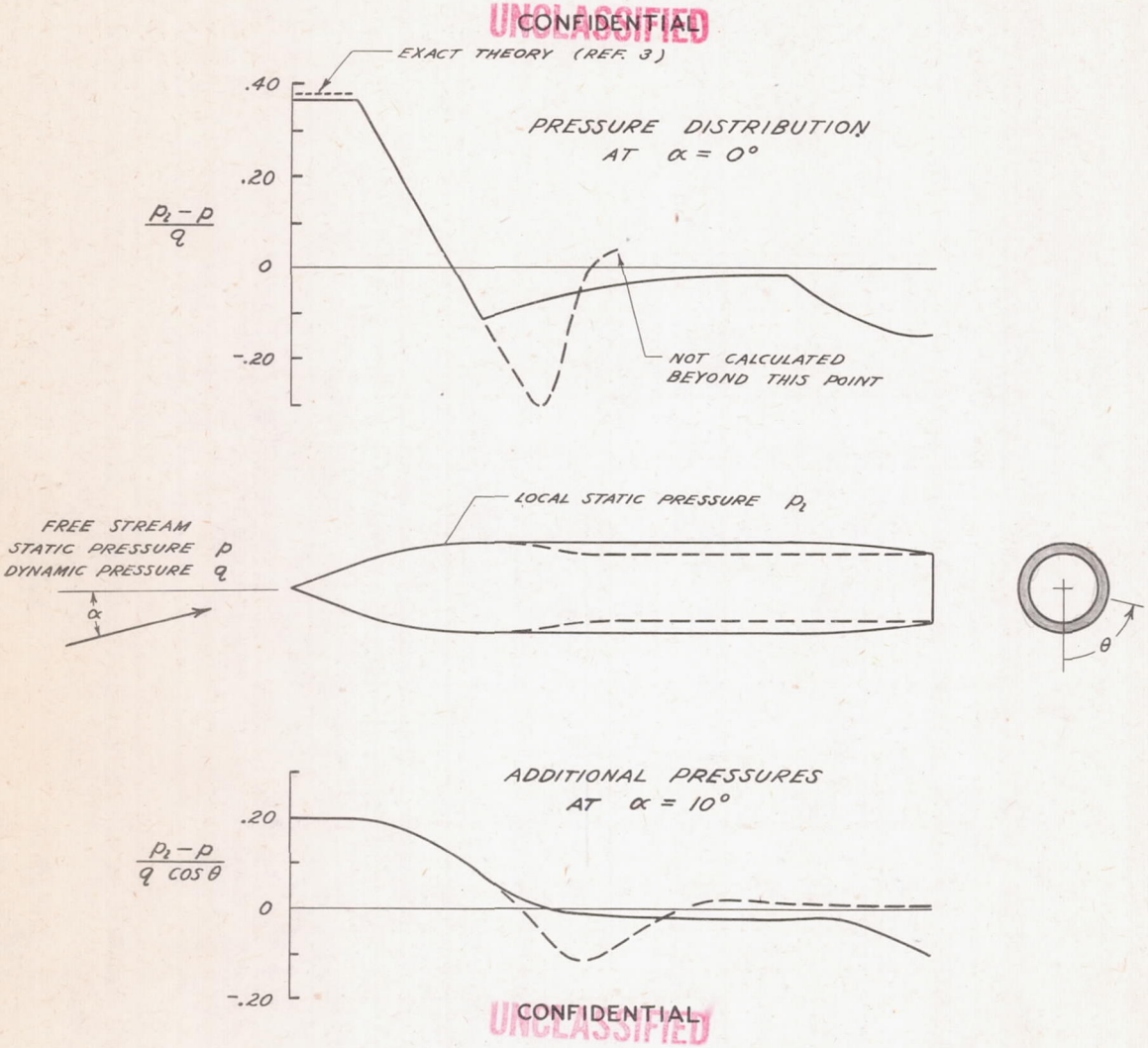

NATIONAL ADVISORY
COMMITTEE FOR AERONAUTICS

FIGURE 9. - THEORETICAL PRESSURE DISTRIBUTIONS ON BASIC AND BULBOUS BODIES AT 1.53 MACH NUMBER

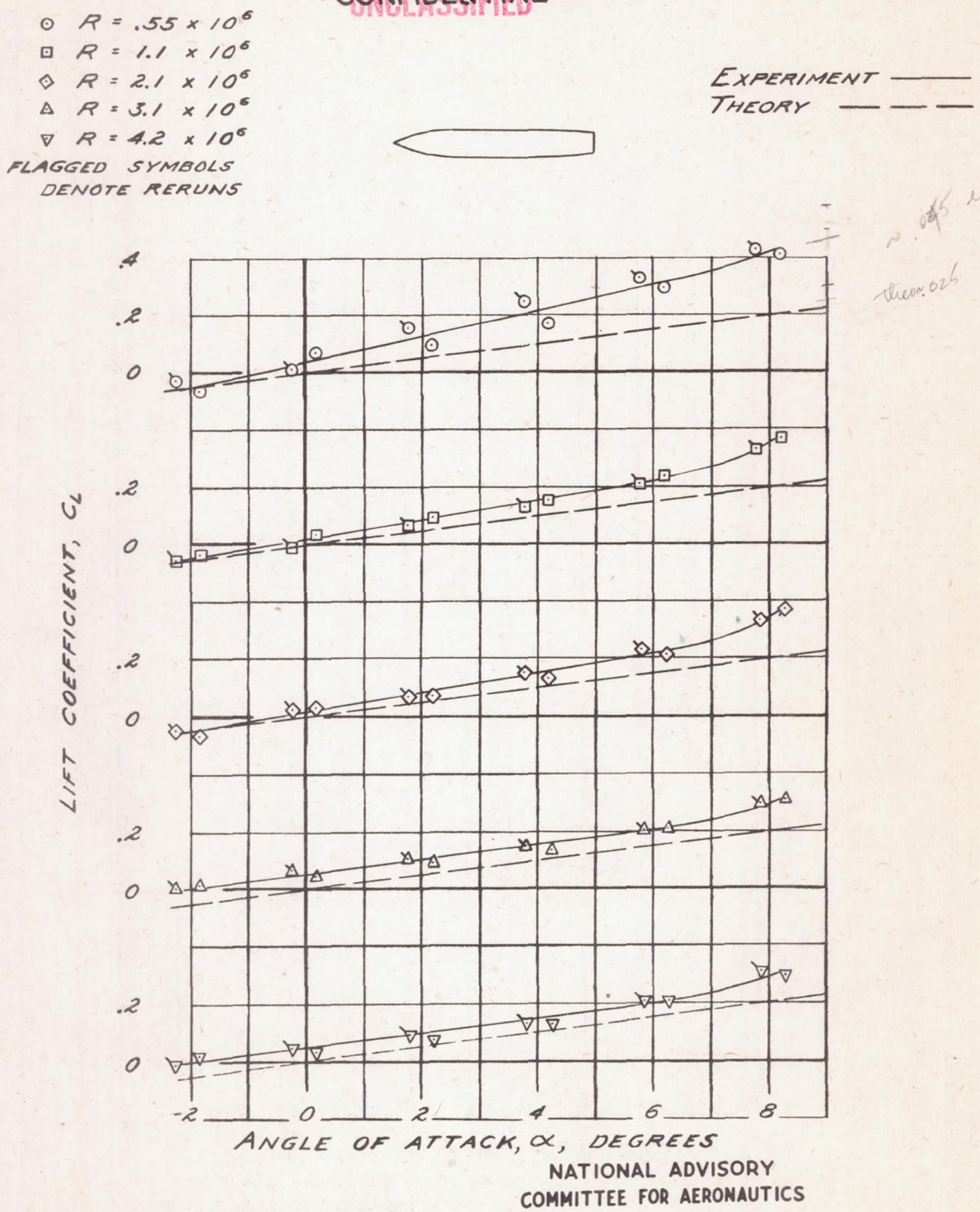

(a) BASIC BODY

FIGURE 10.- VARIATION OF LIFT COEFFICIENT WITH ANGLE OF ATTACK FOR BODIES.

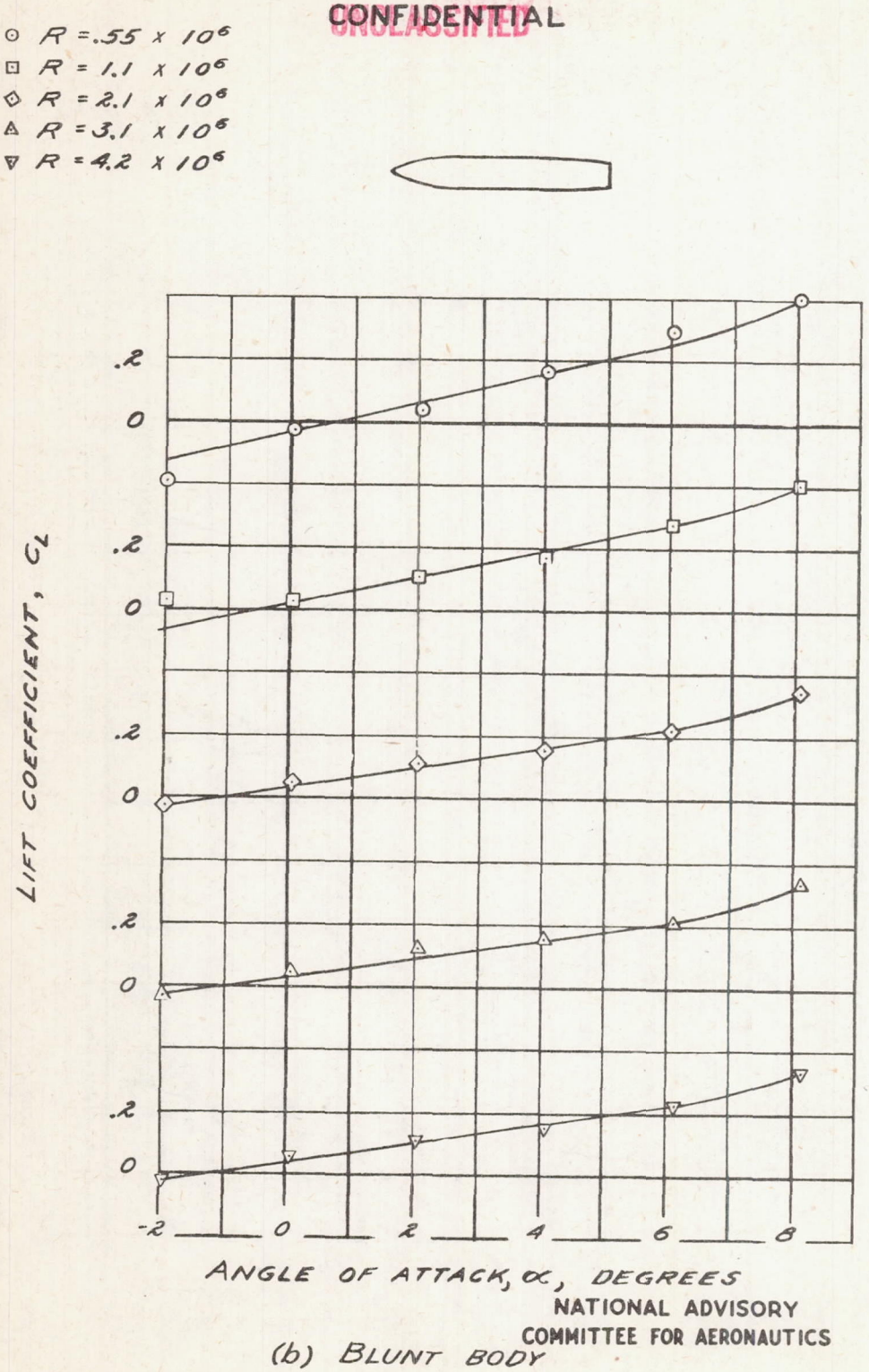

(b) BLUNT BODY

FIGURE 10.- CONTINUED.

⊙ $R = .55 \times 10^6$
⊡ $R = 1.1 \times 10^6$
◇ $R = 2.1 \times 10^6$
△ $R = 3.1 \times 10^6$
▽ $R = 4.2 \times 10^6$

EXPERIMENT ——
THEORY — — —

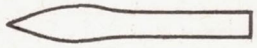

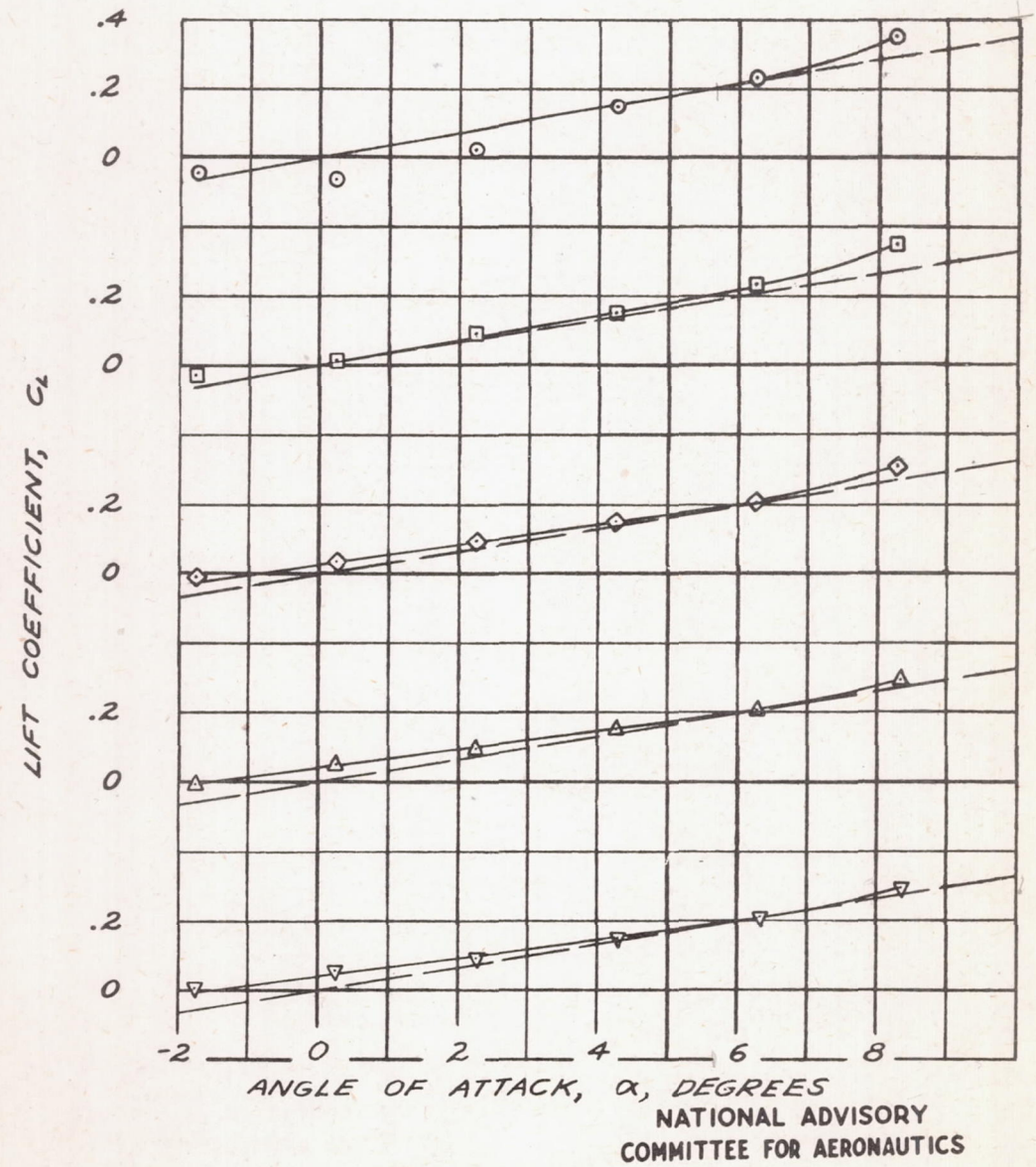

(c) BULBOUS BODY

FIGURE 10.- CONCLUDED.

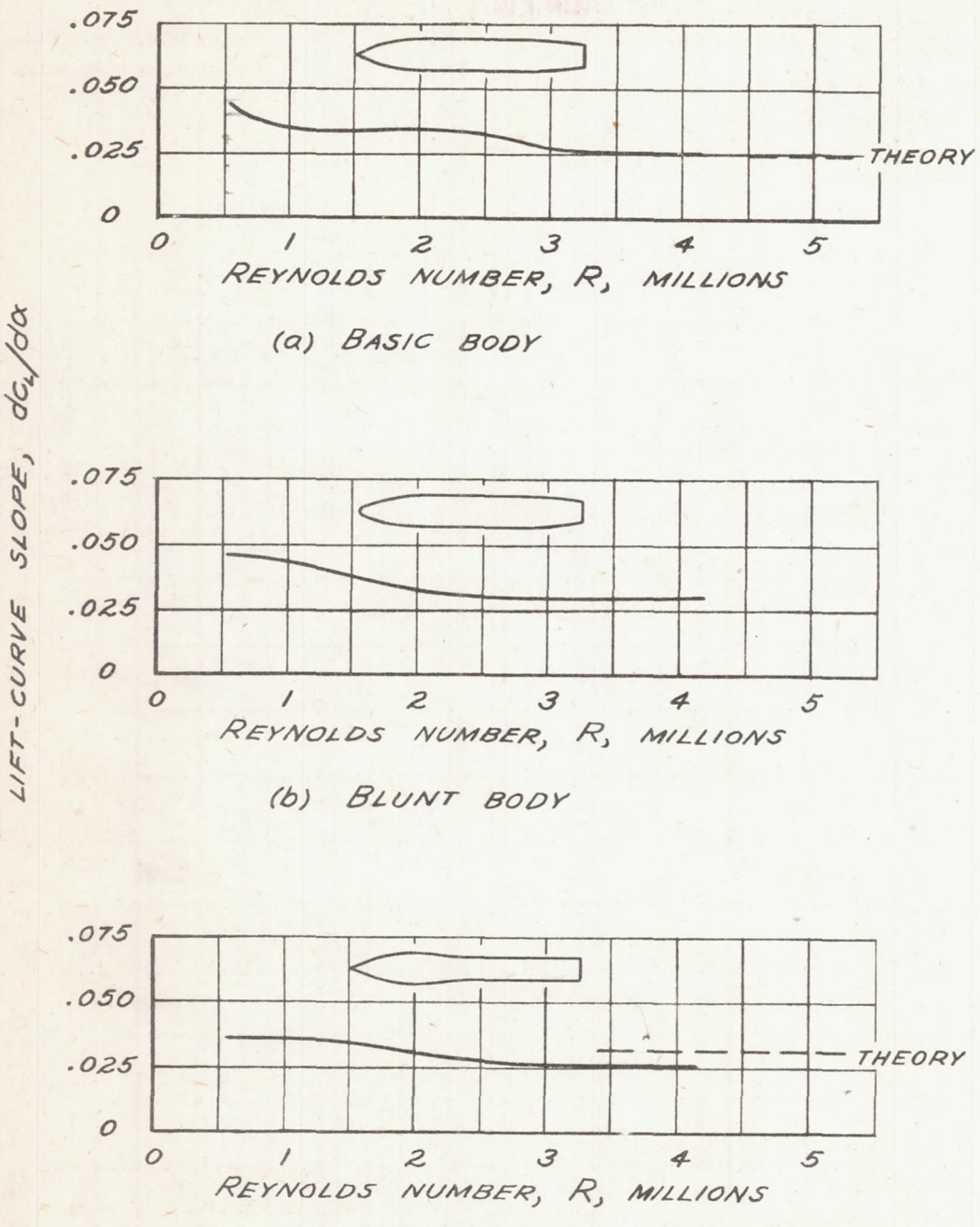

NATIONAL ADVISORY
COMMITTEE FOR AERONAUTICS

FIGURE 11. - VARIATION OF LIFT-CURVE SLOPE WITH REYNOLDS NUMBER FOR BODIES

CONFIDENTIAL

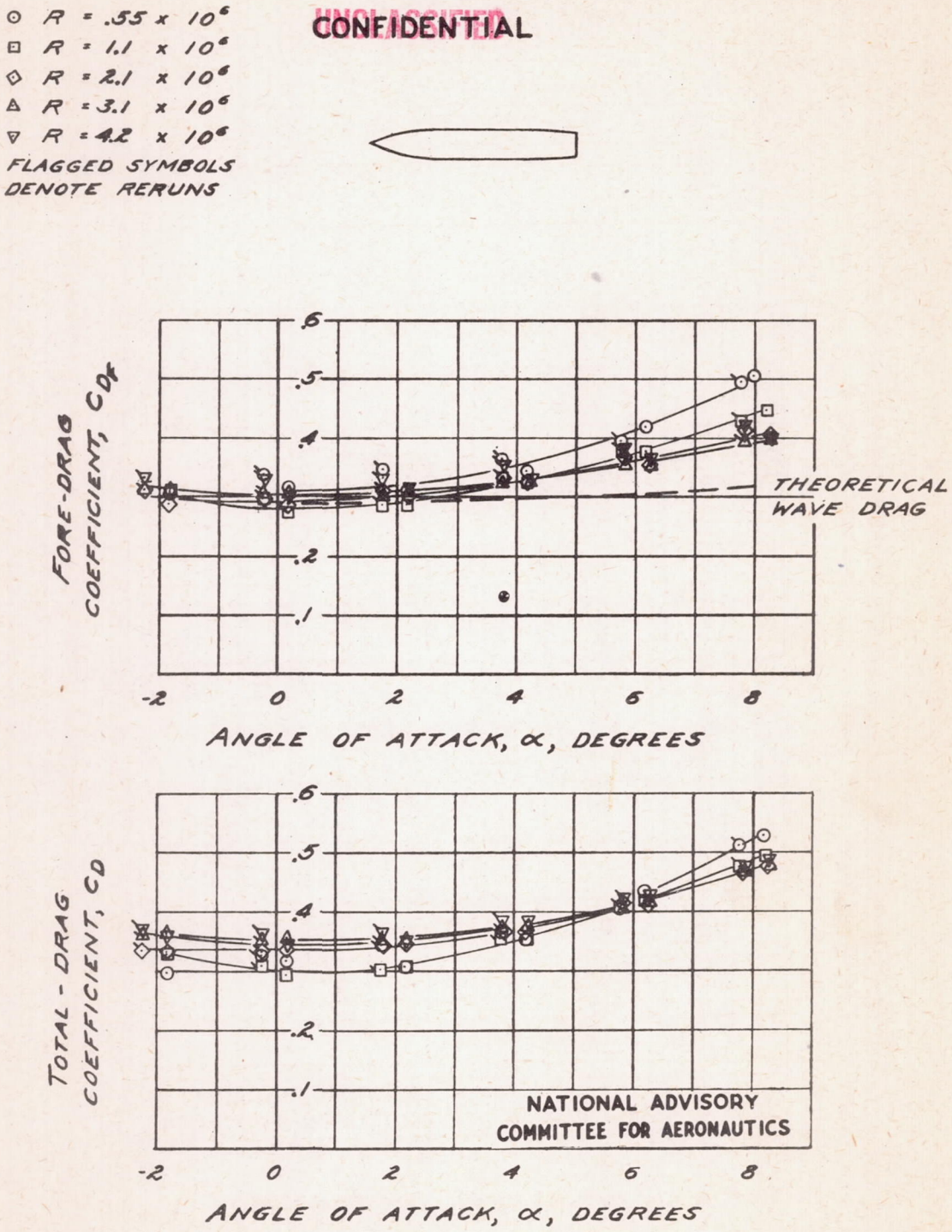

(a) BASIC BODY

FIGURE 12. - VARIATION OF TOTAL-DRAG AND FORE-DRAG COEFFICIENTS WITH ANGLE OF ATTACK FOR BODIES.

CONFIDENTIAL

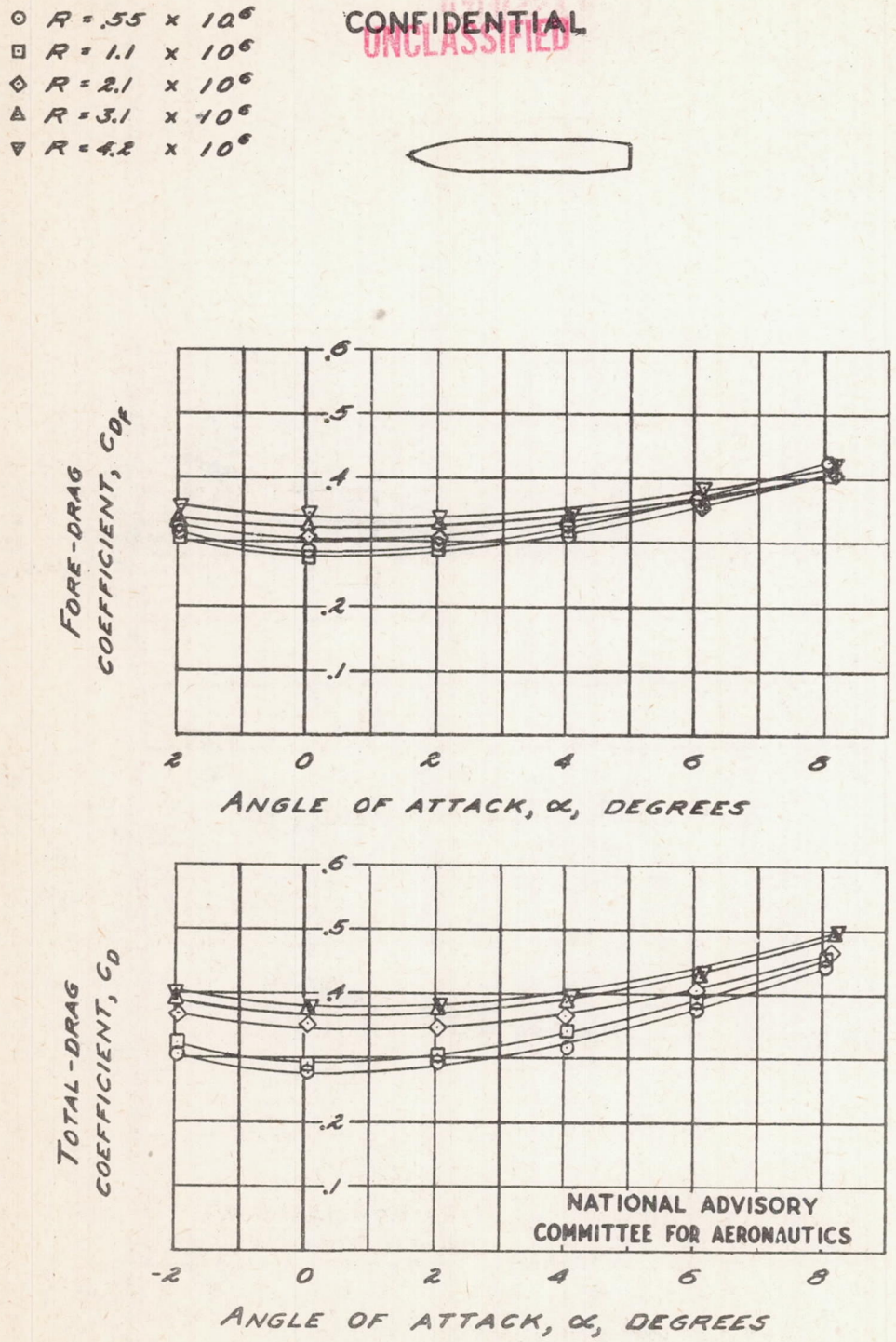

(b) BLUNT BODY

FIGURE 12. - CONTINUED.

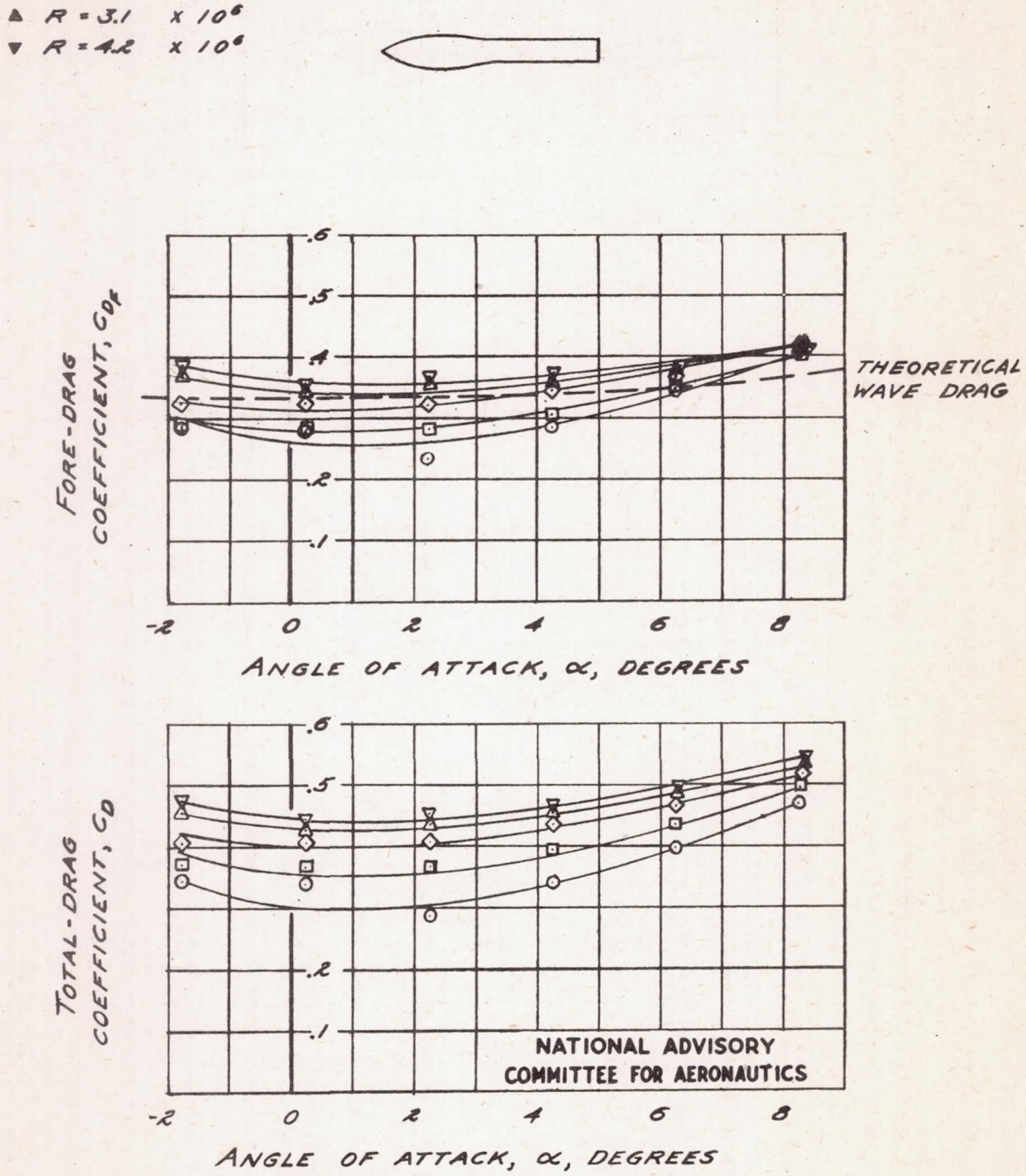

(c) Bulbous body

FIGURE 12. - CONCLUDED.

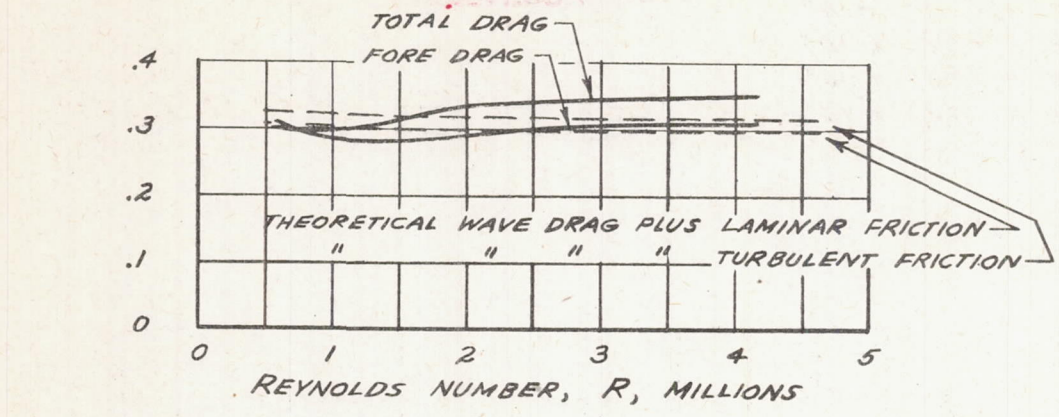

(a) BASIC BODY

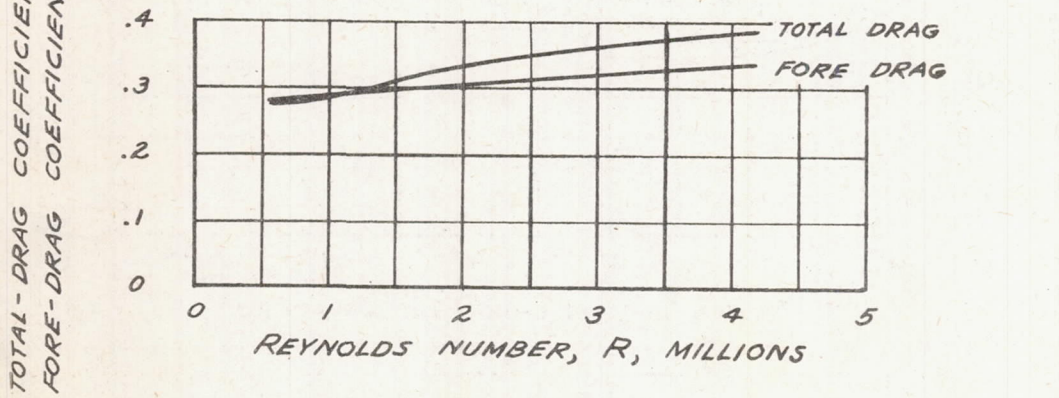

(b) BLUNT BODY

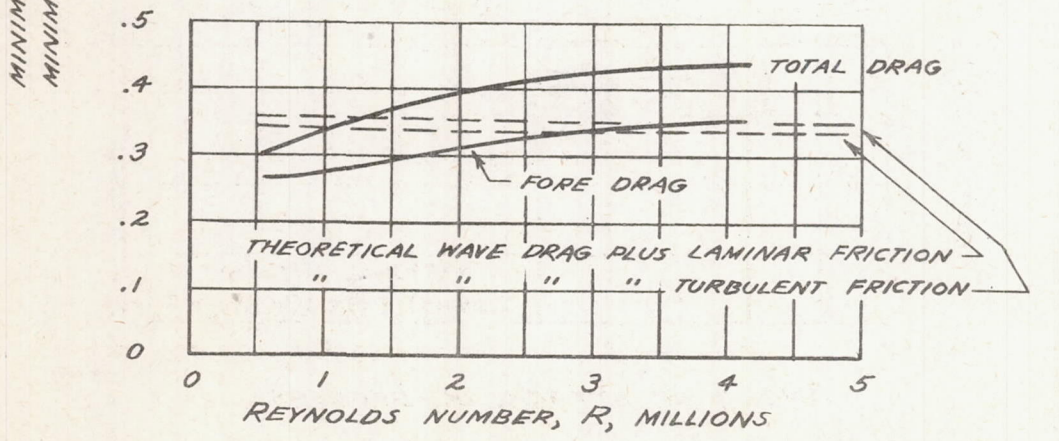

(c) BULBOUS BODY

NATIONAL ADVISORY
COMMITTEE FOR AERONAUTICS

FIGURE 13. - VARIATION OF MINIMUM TOTAL-DRAG AND FORE-DRAG COEFFICIENTS WITH REYNOLDS NUMBER FOR BODIES.

CONFIDENTIAL

⊙ $R = .55 \times 10^6$
⊡ $R = 1.1 \times 10^6$
◇ $R = 2.1 \times 10^6$
△ $R = 3.1 \times 10^6$
▽ $R = 4.2 \times 10^6$

EXPERIMENT ———
THEORY — — —

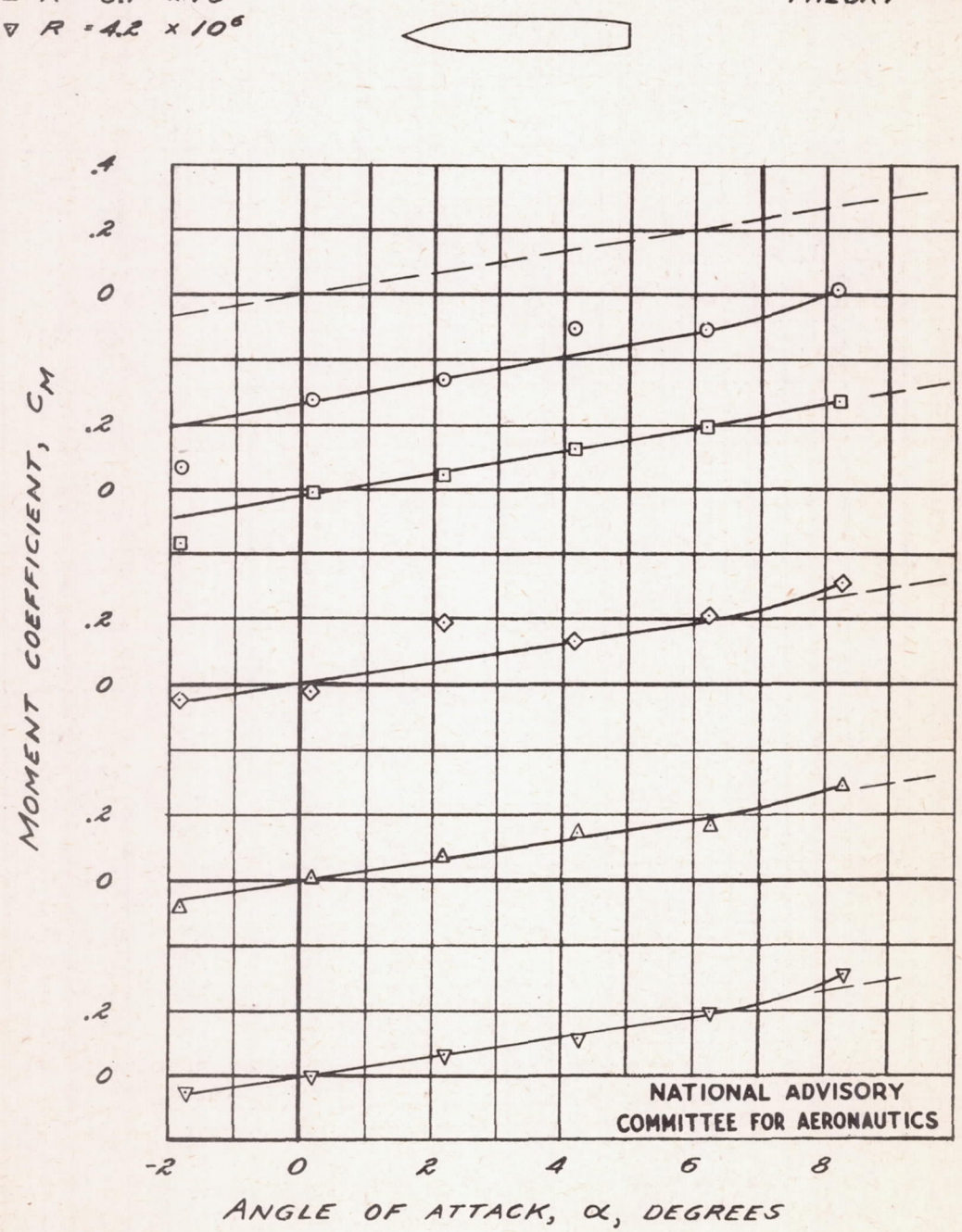

FIGURE 14.- VARIATION OF PITCHING-MOMENT COEFFICIENT WITH ANGLE OF ATTACK FOR BASIC BODY.

CONFIDENTIAL

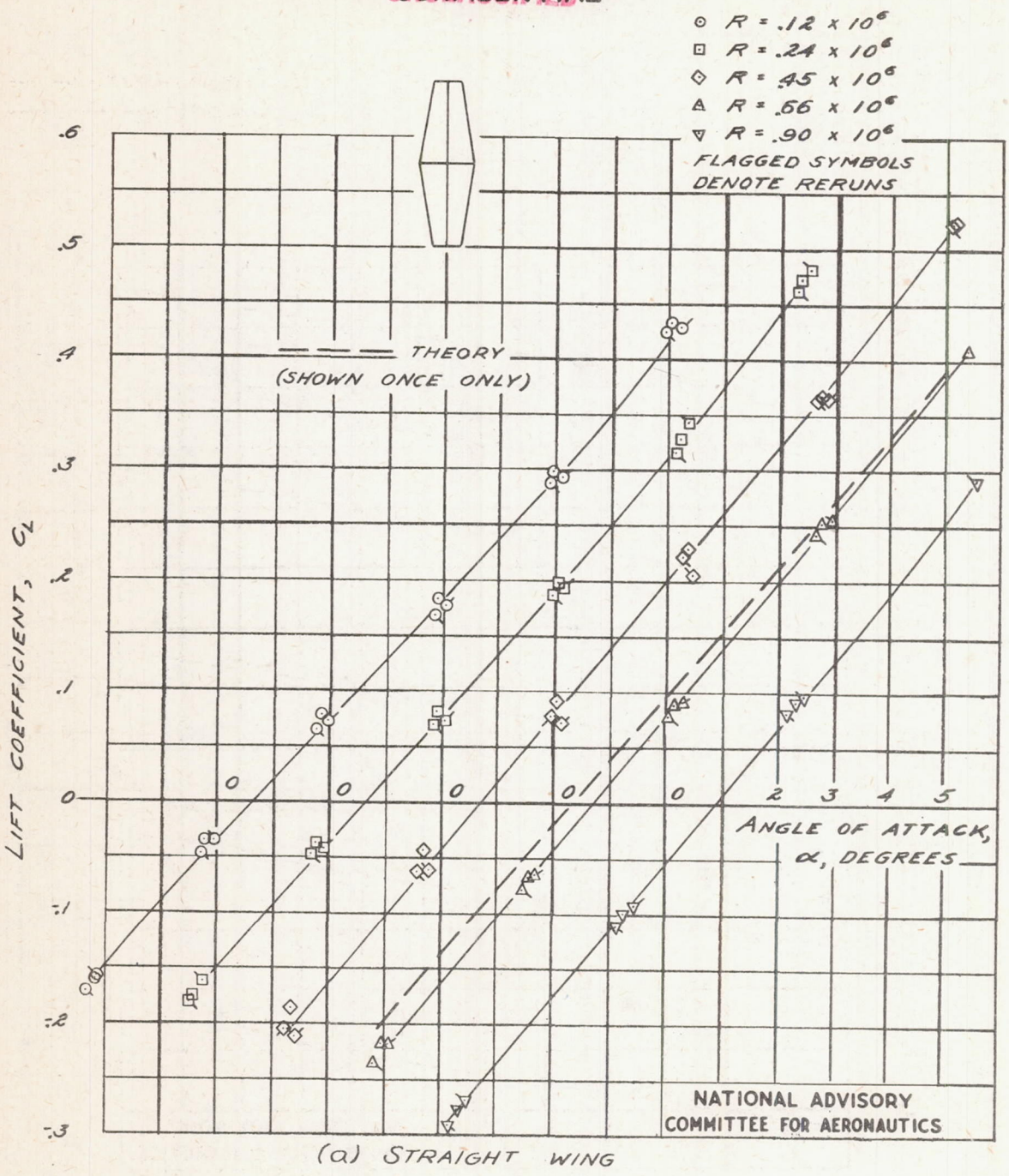

(a) STRAIGHT WING

FIGURE 15. - VARIATION OF LIFT COEFFICIENT WITH ANGLE OF ATTACK FOR WINGS

CONFIDENTIAL

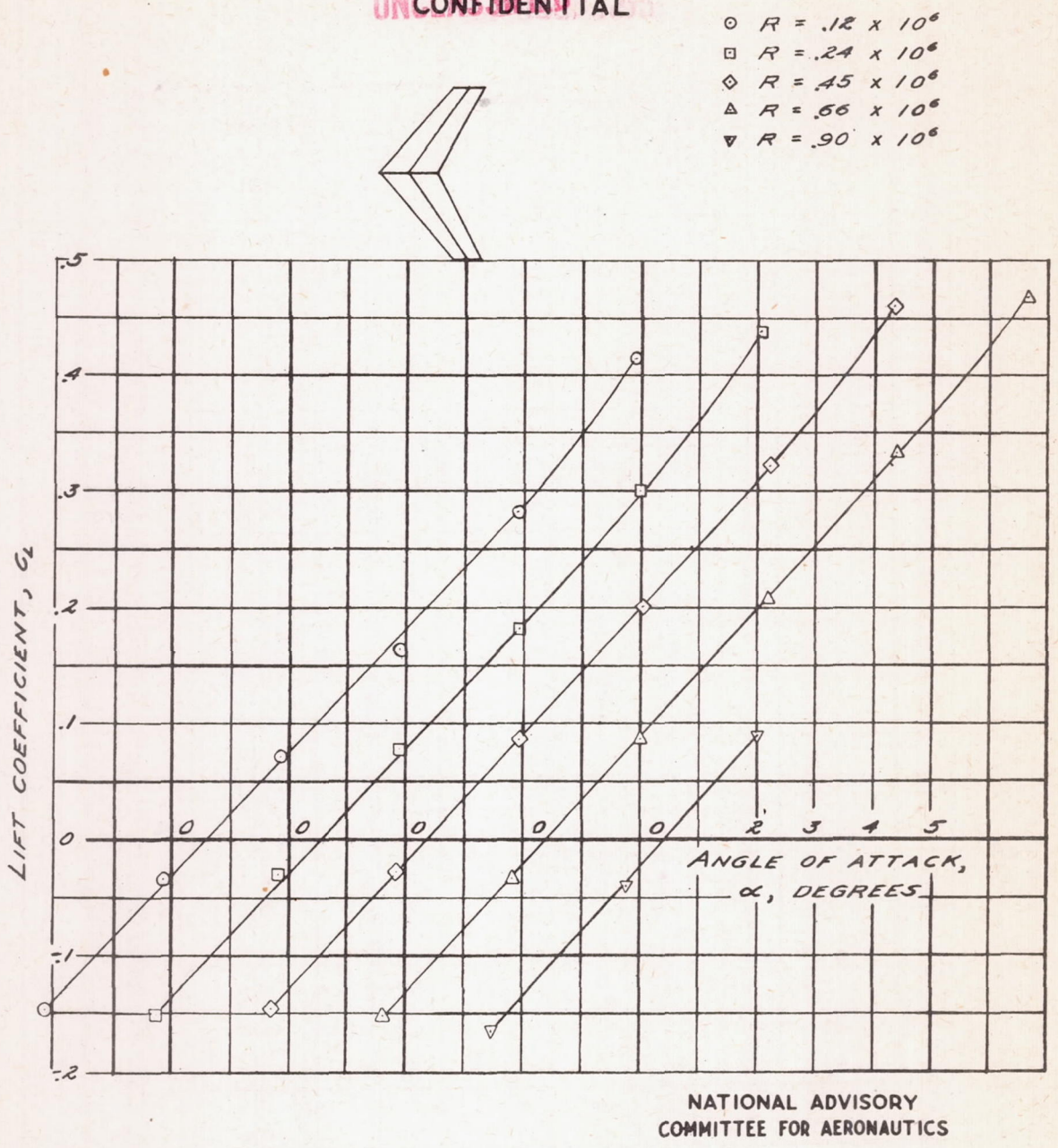

(b) SWEPTBACK WING

FIGURE 15.- CONCLUDED.

CONFIDENTIAL

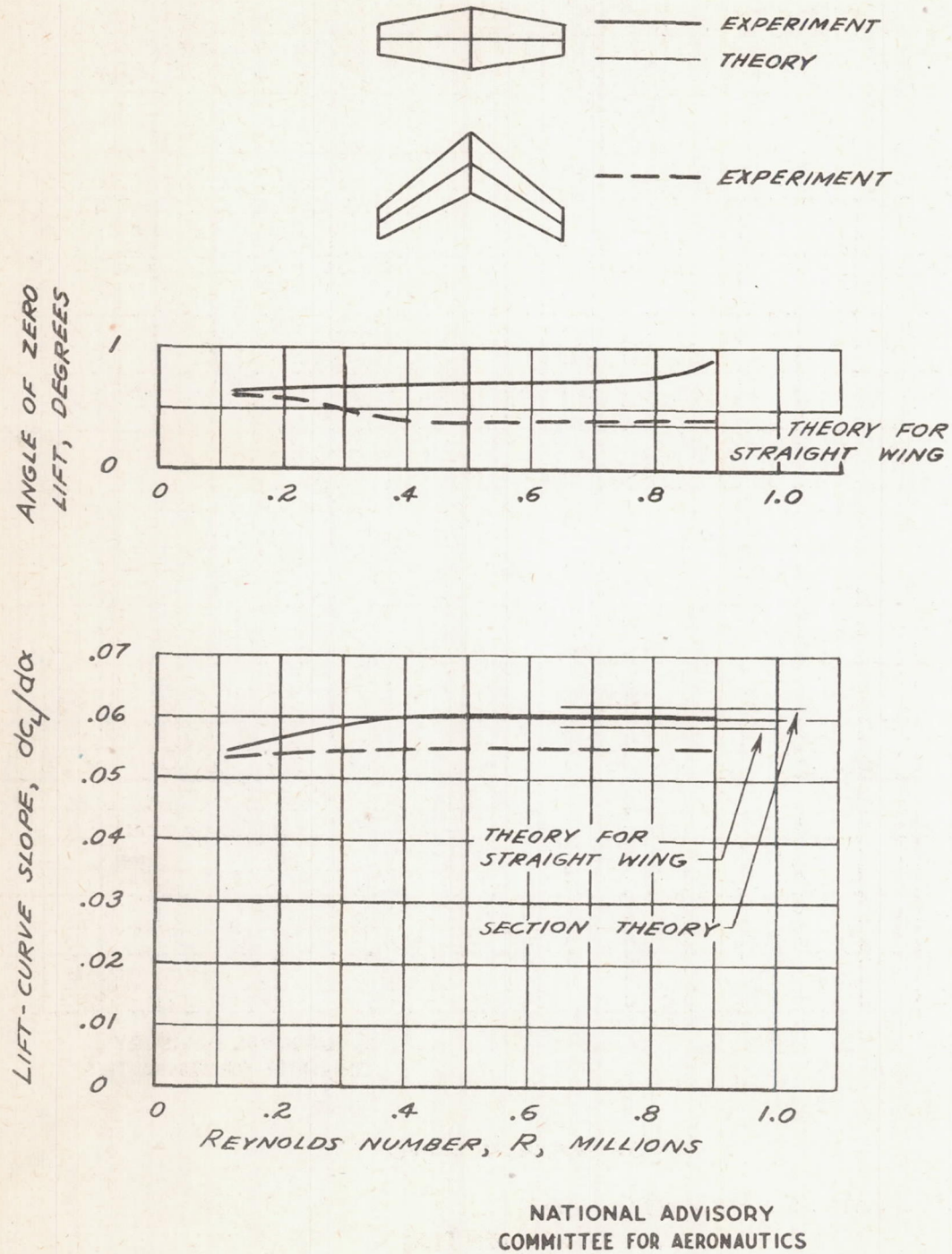

NATIONAL ADVISORY
COMMITTEE FOR AERONAUTICS

FIGURE 16. - VARIATION OF ANGLE OF ZERO LIFT AND LIFT-CURVE SLOPE WITH REYNOLDS NUMBER FOR STRAIGHT AND SWEPTBACK WINGS.

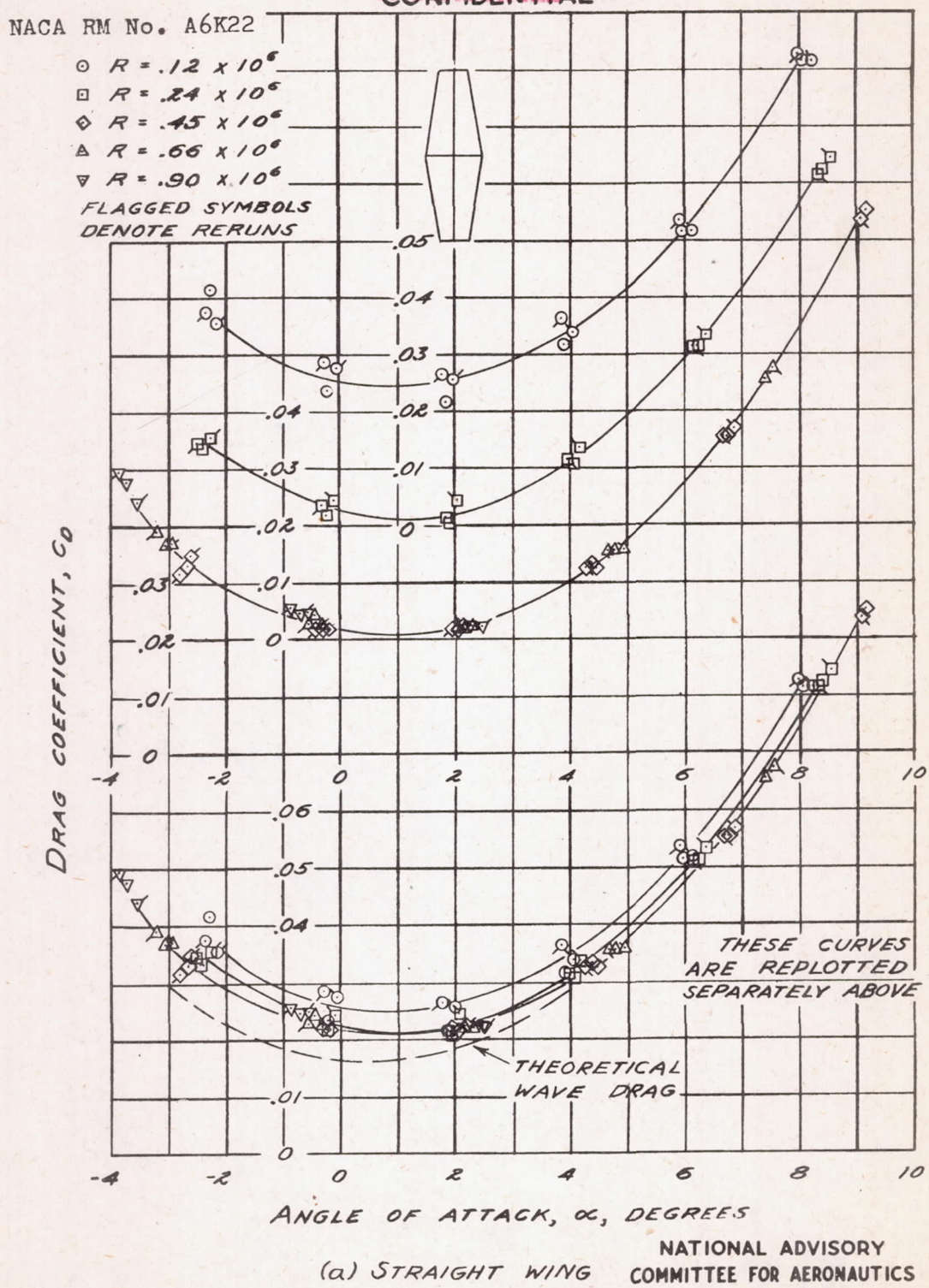

(a) STRAIGHT WING

FIGURE 17. - VARIATION OF DRAG COEFFICIENT WITH ANGLE OF ATTACK FOR WINGS.

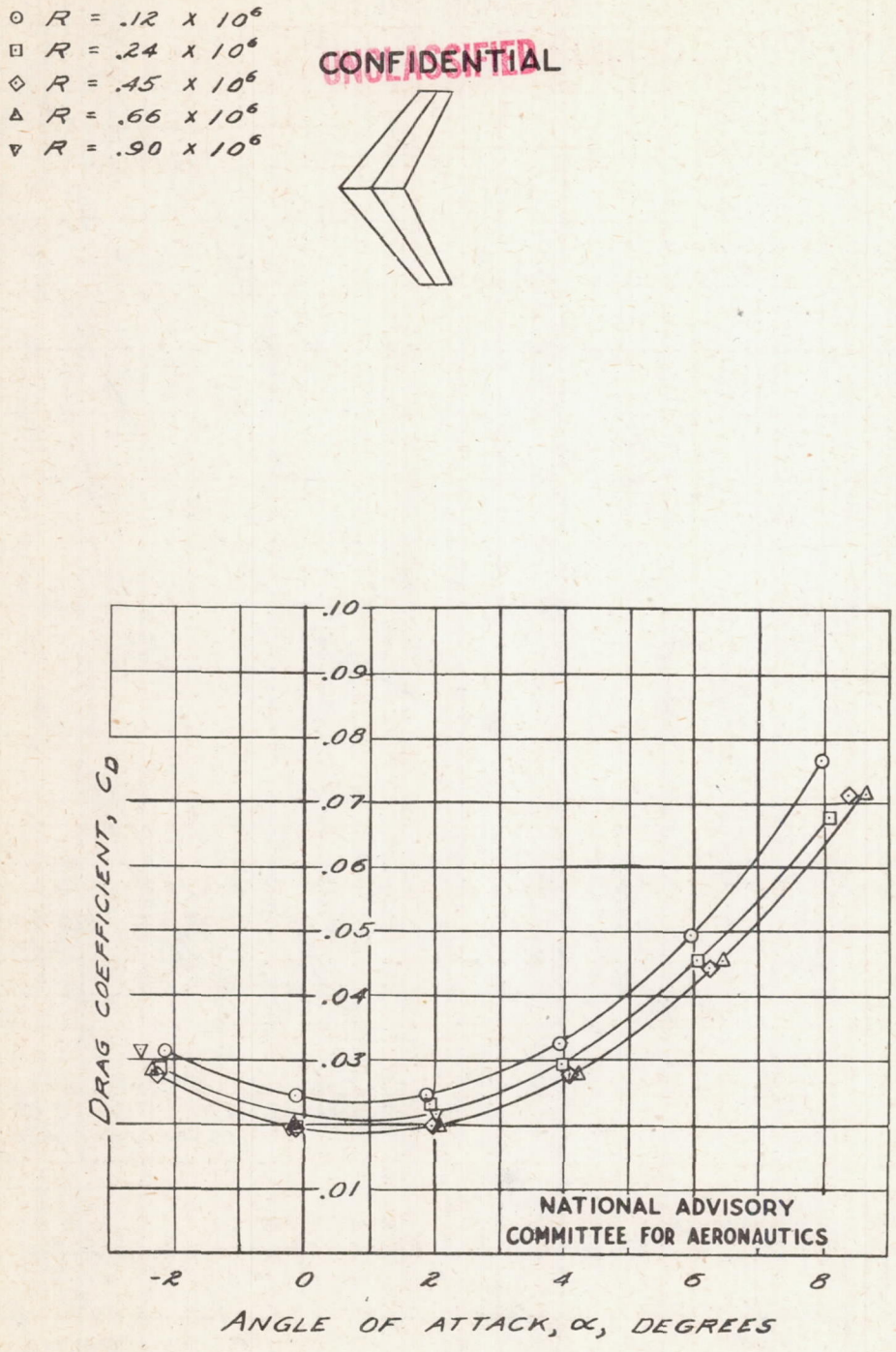

(b) SWEPTBACK WING

FIGURE 17. - CONCLUDED.

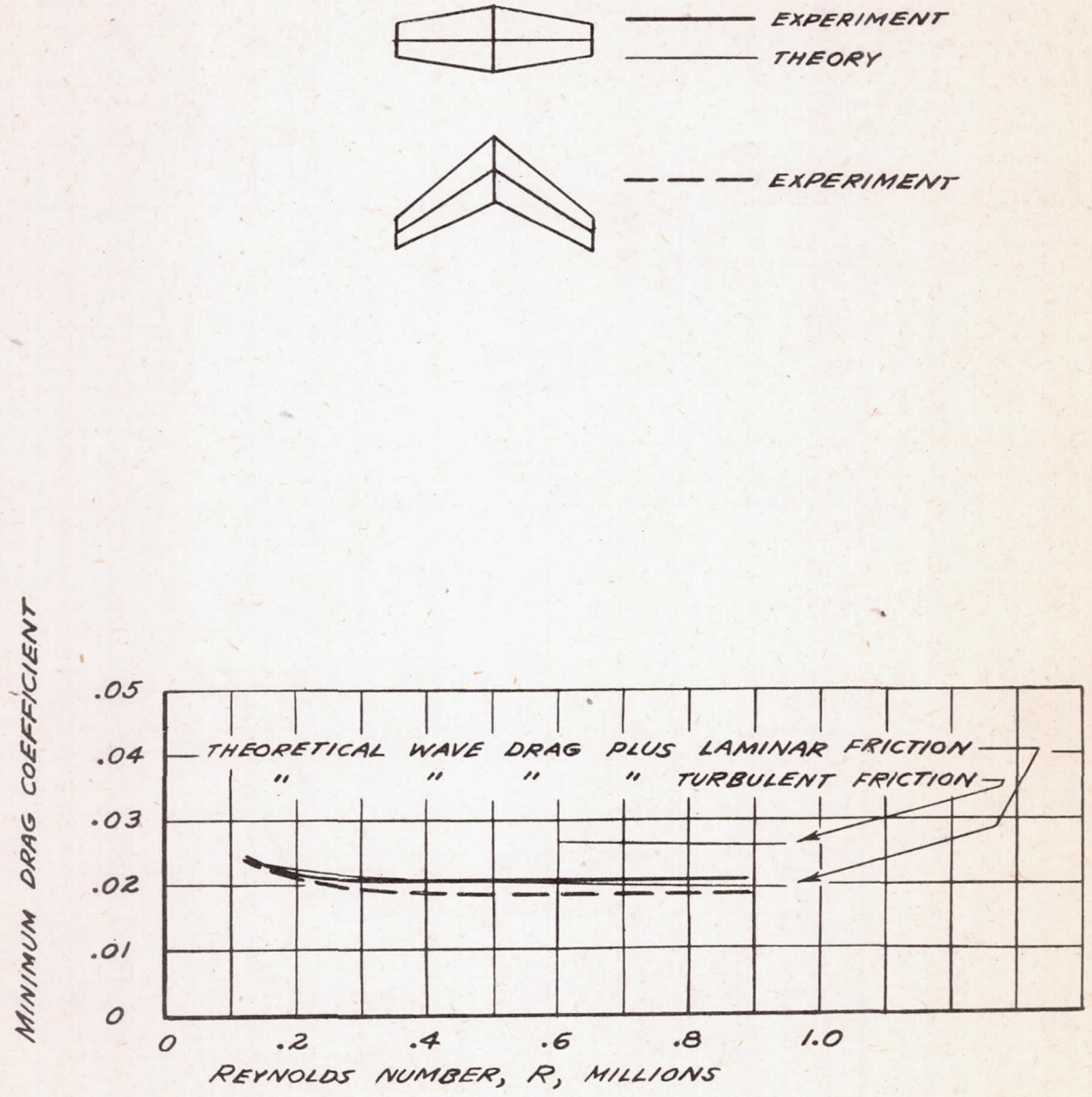

NATIONAL ADVISORY
COMMITTEE FOR AERONAUTIC

FIGURE 18. - VARIATION OF MINIMUM DRAG COEFFICIENT WITH REYNOLDS NUMBER FOR STRAIGHT AND SWEPTBACK WINGS.

CONFIDENTIAL

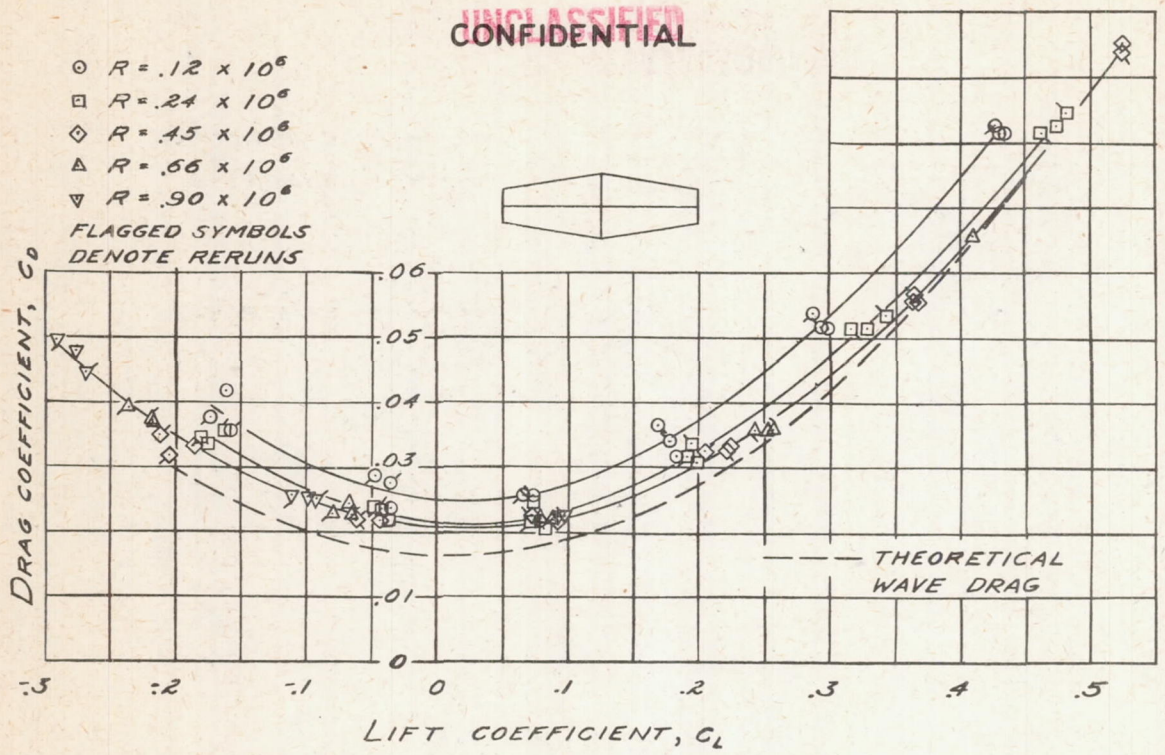

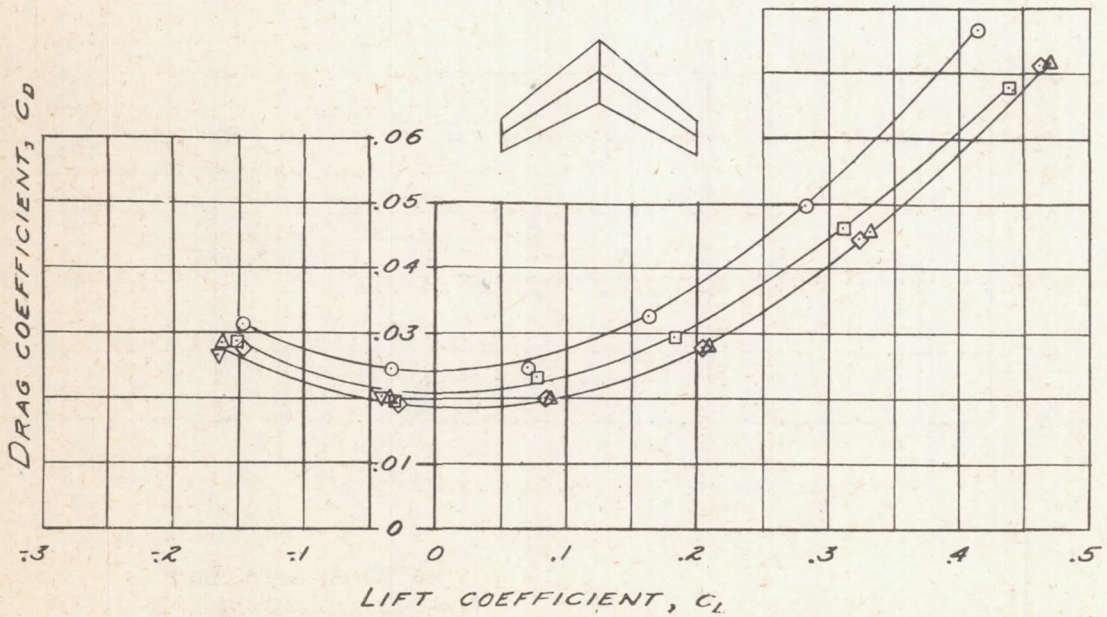

NATIONAL ADVISORY
COMMITTEE FOR AERONAUTICS

FIGURE 19.- VARIATION OF DRAG COEFFICIENT WITH LIFT COEFFICIENT FOR STRAIGHT AND SWEPTBACK WINGS.

CONFIDENTIAL

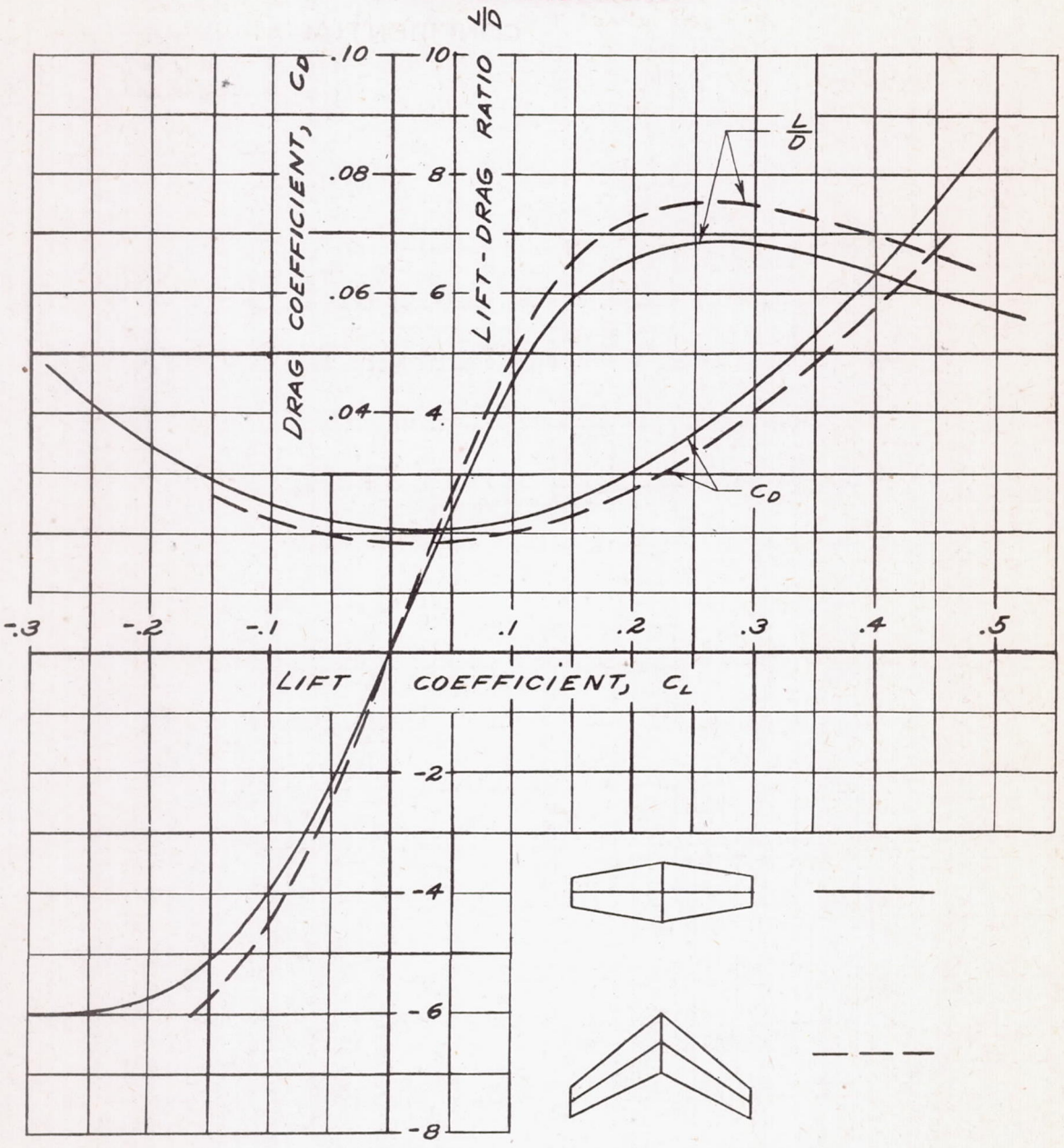

FIGURE 20.- VARIATION OF DRAG COEFFICIENT AND LIFT-DRAG RATIO WITH LIFT COEFFICIENT FOR STRAIGHT AND SWEPTBACK WINGS ABOVE ONE-HALF MILLION REYNOLDS NUMBER

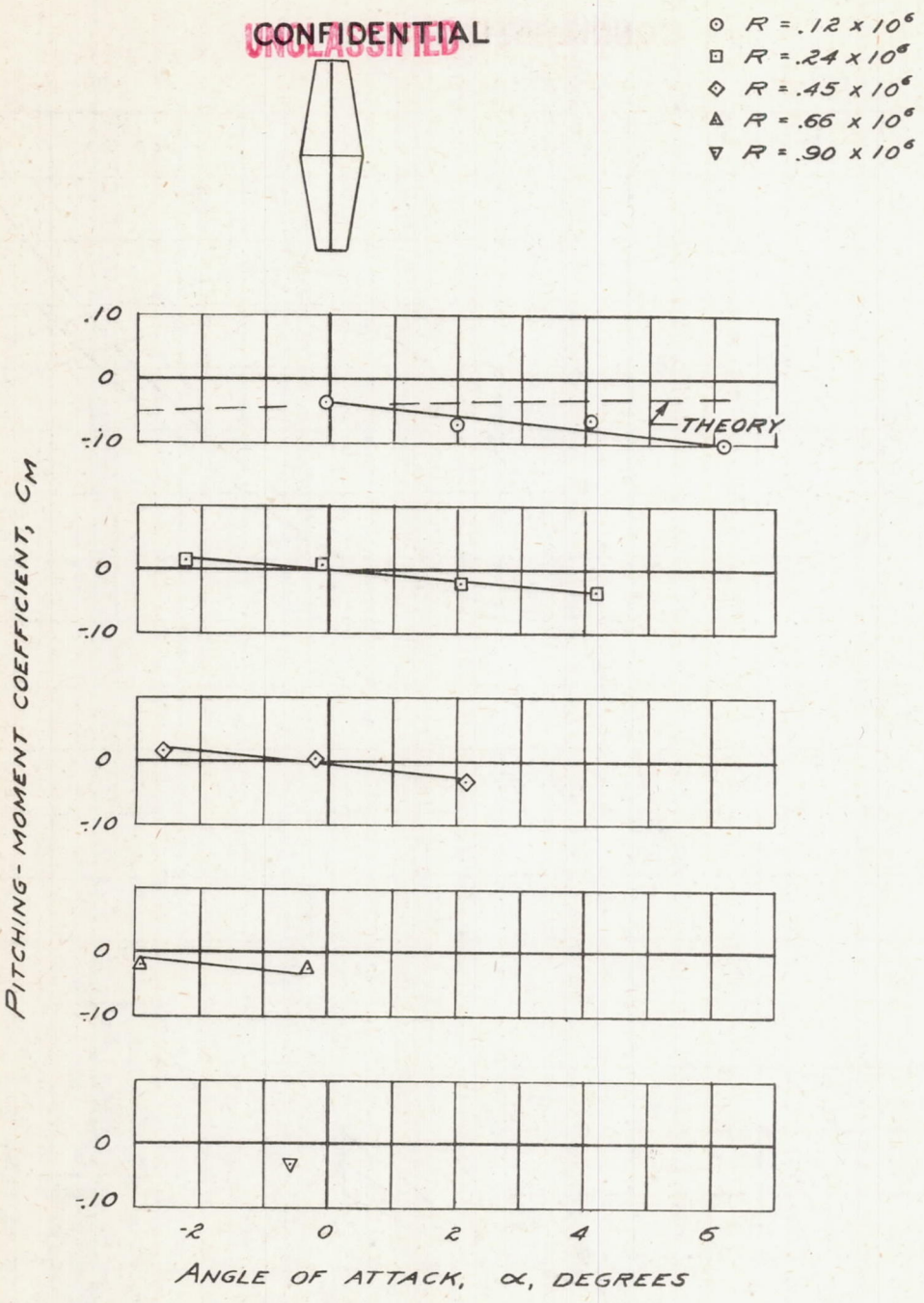

(a) STRAIGHT WING

NATIONAL ADVISORY COMMITTEE FOR AERONAUTICS

FIGURE 21. - VARIATION OF PITCHING-MOMENT COEFFICIENT WITH ANGLE OF ATTACK FOR WINGS.

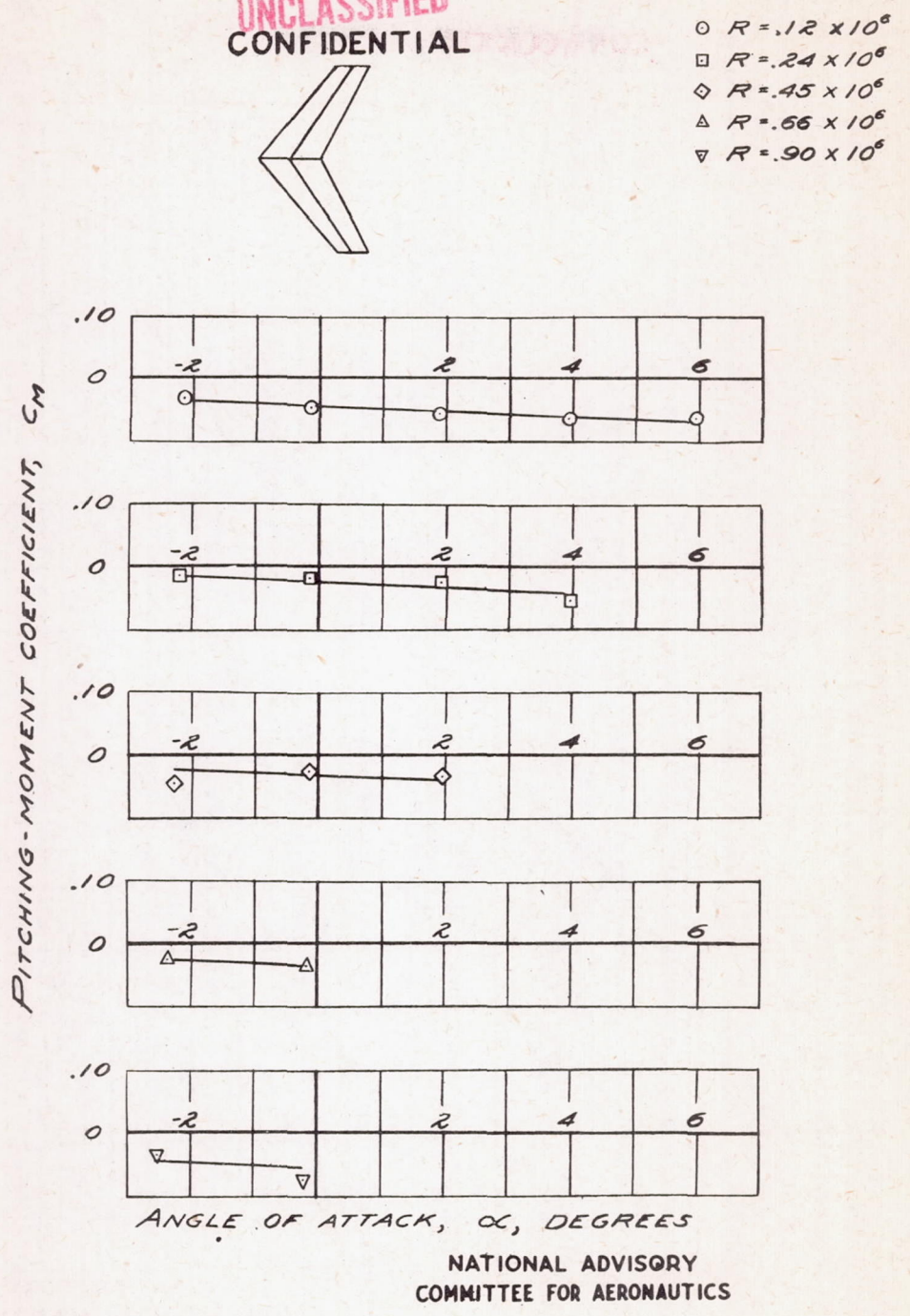

(b) SWEPTBACK WING

FIGURE 21. - CONCLUDED.

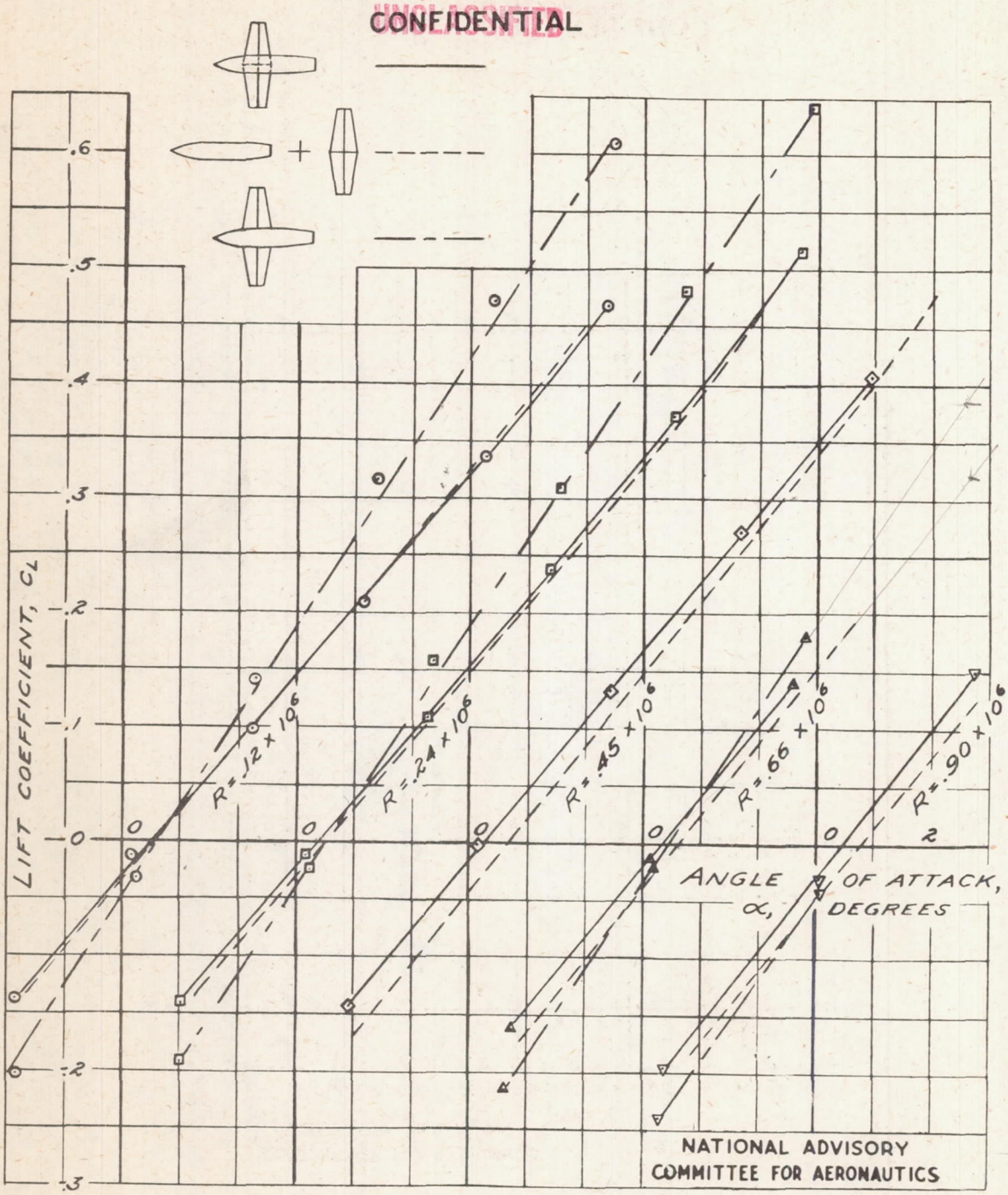

(a) Basic body, straight wing planform.

Figure 22. - Lift curves for wing-body combinations compared with sum of lift curves for components.

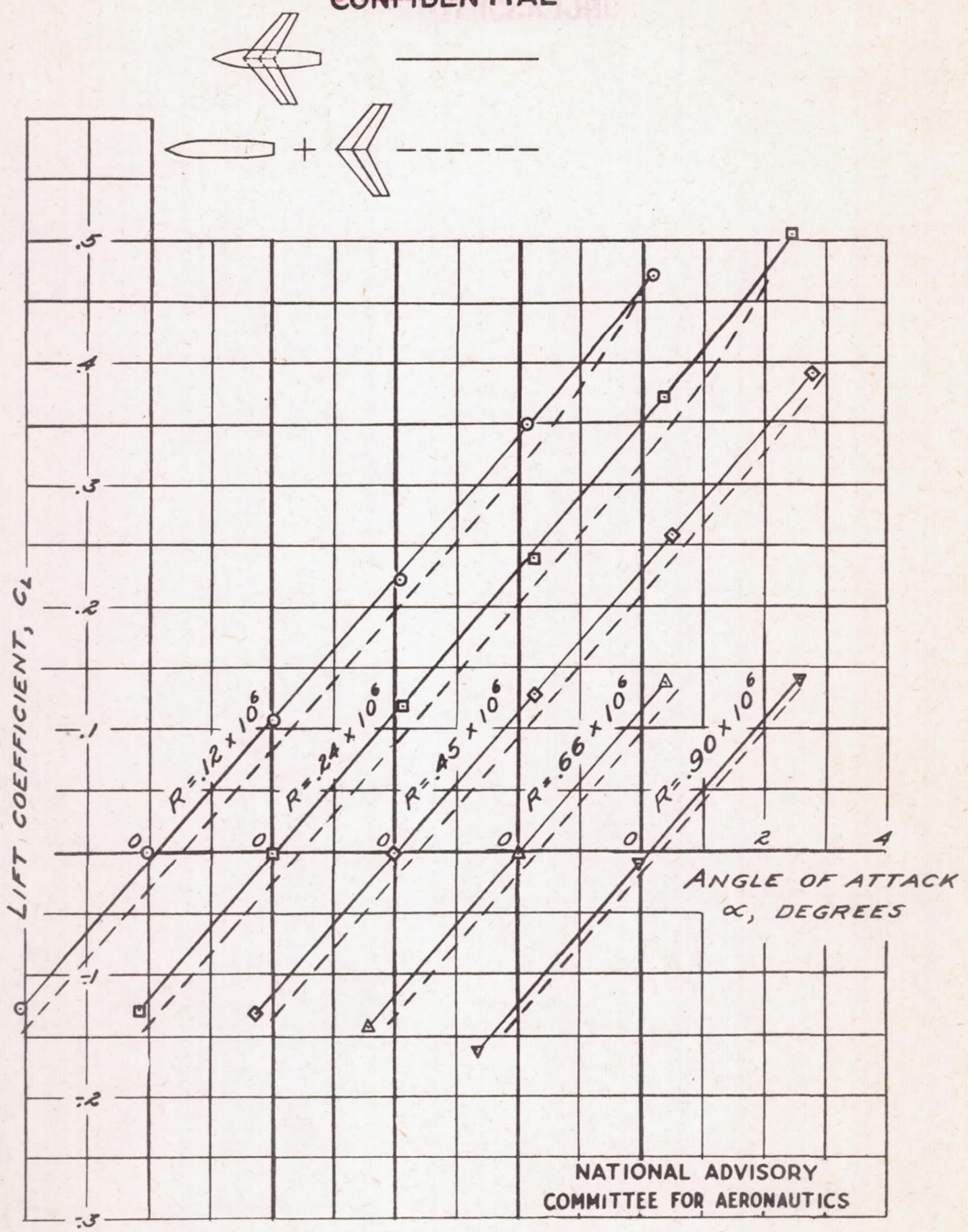

(b) BASIC BODY, SWEPTBACK WING PLANFORM.

FIGURE 22. - CONTINUED.

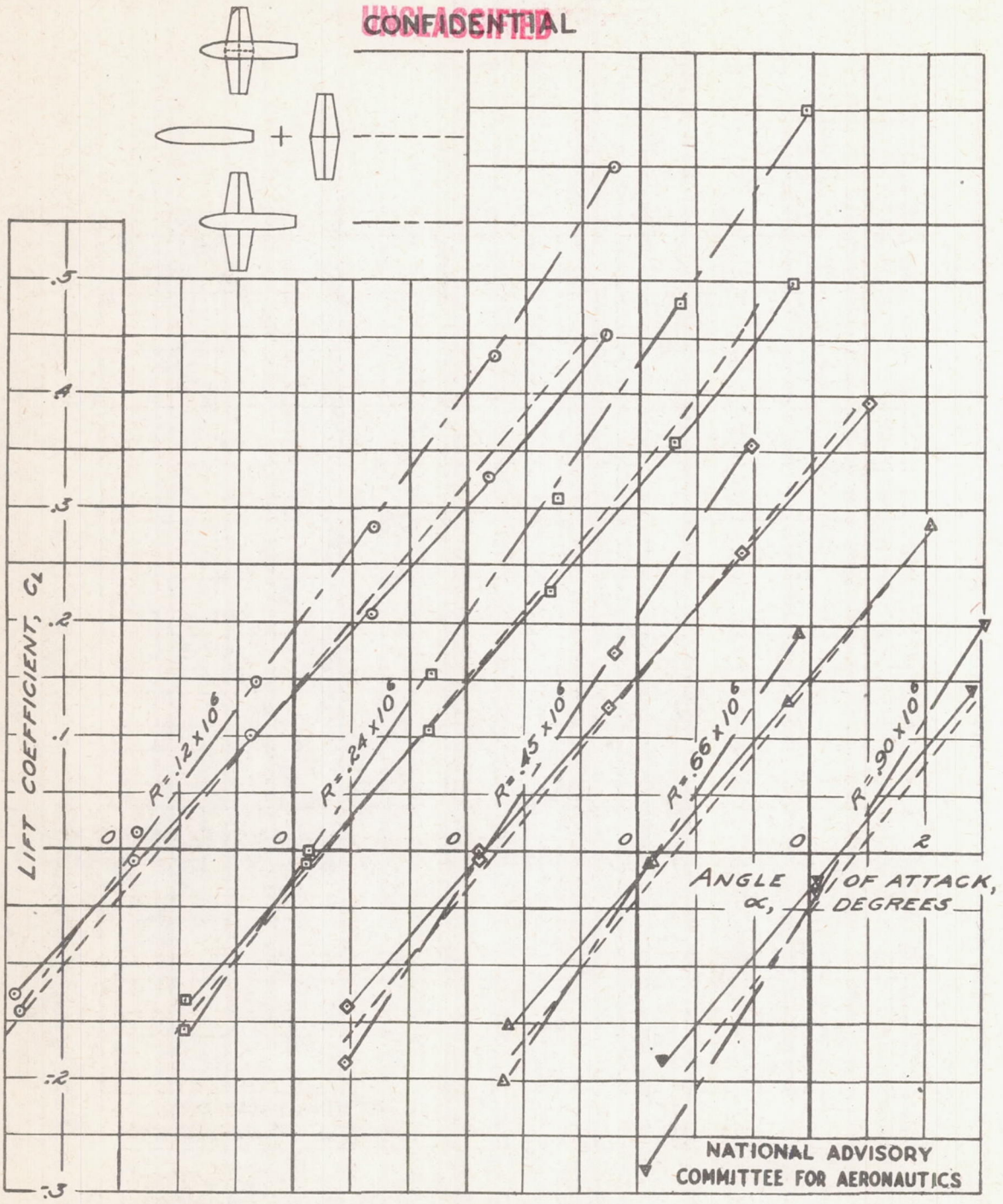

(c) BLUNT BODY, STRAIGHT WING PLANFORM.

FIGURE 22. - CONTINUED.

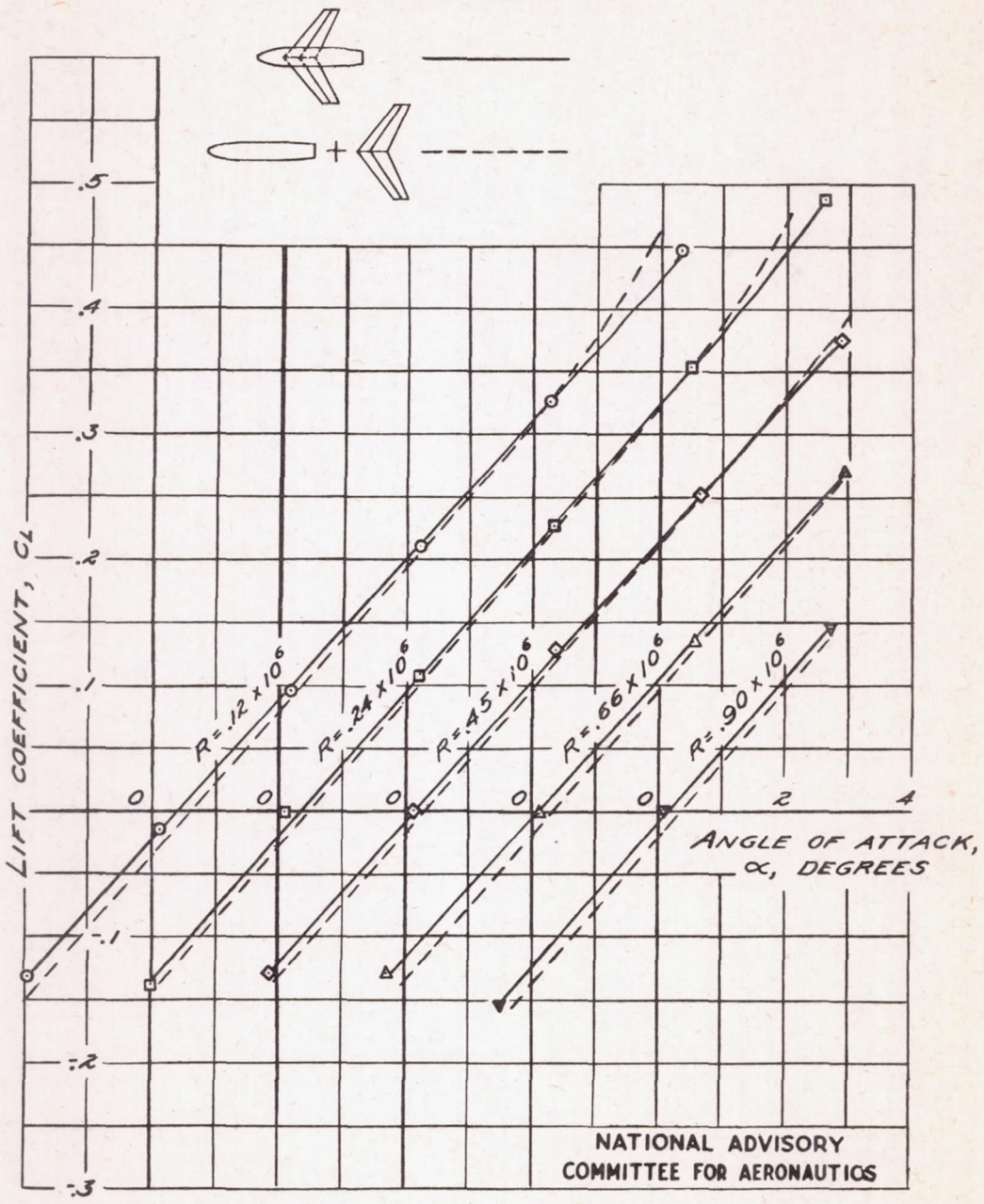

(d) BLUNT BODY, SWEPTBACK WING PLANFORM.

FIGURE 22. - CONTINUED.

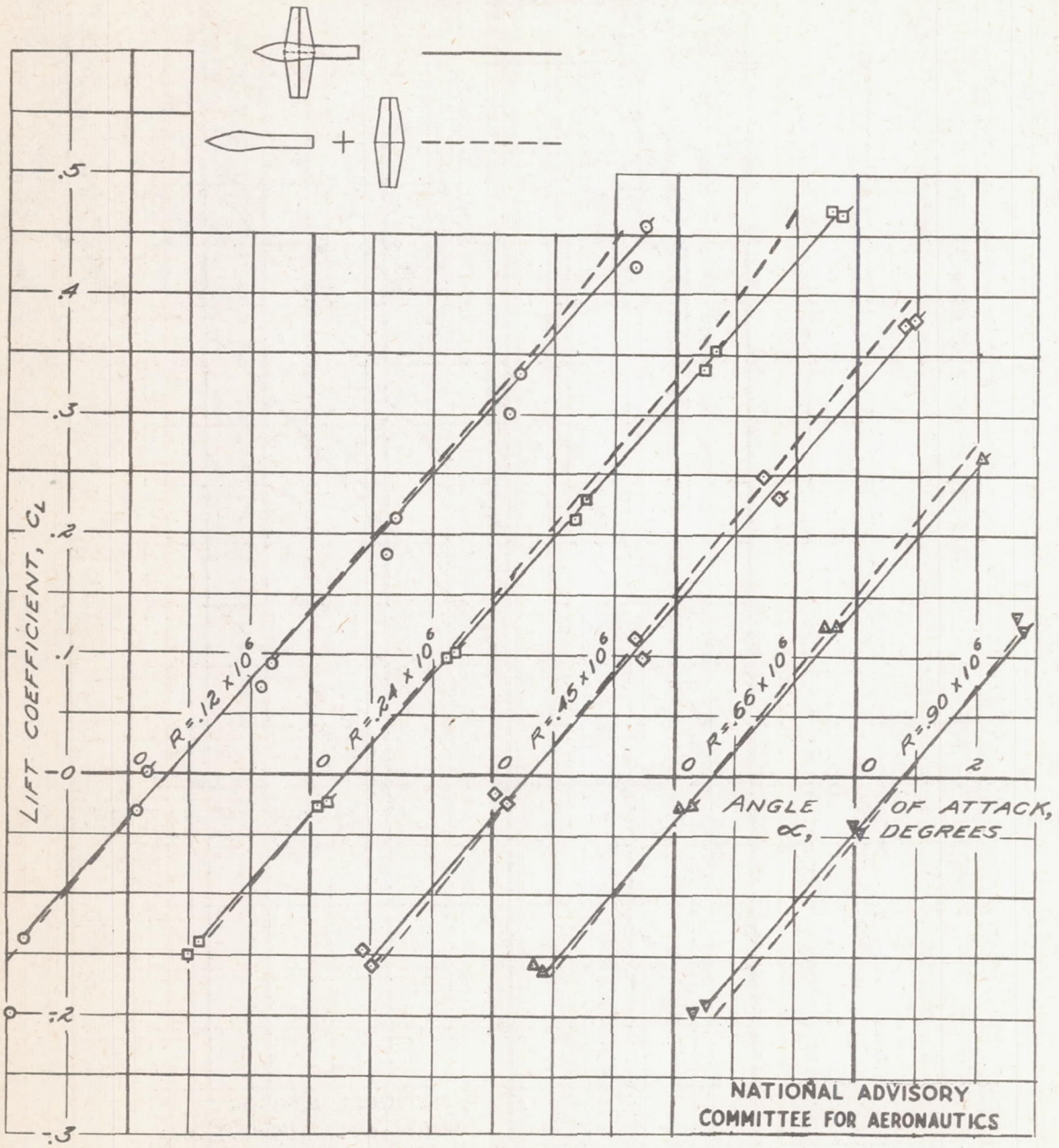

(e) BULBOUS BODY, STRAIGHT WING PLANFORM.

FIGURE 22. - CONTINUED.

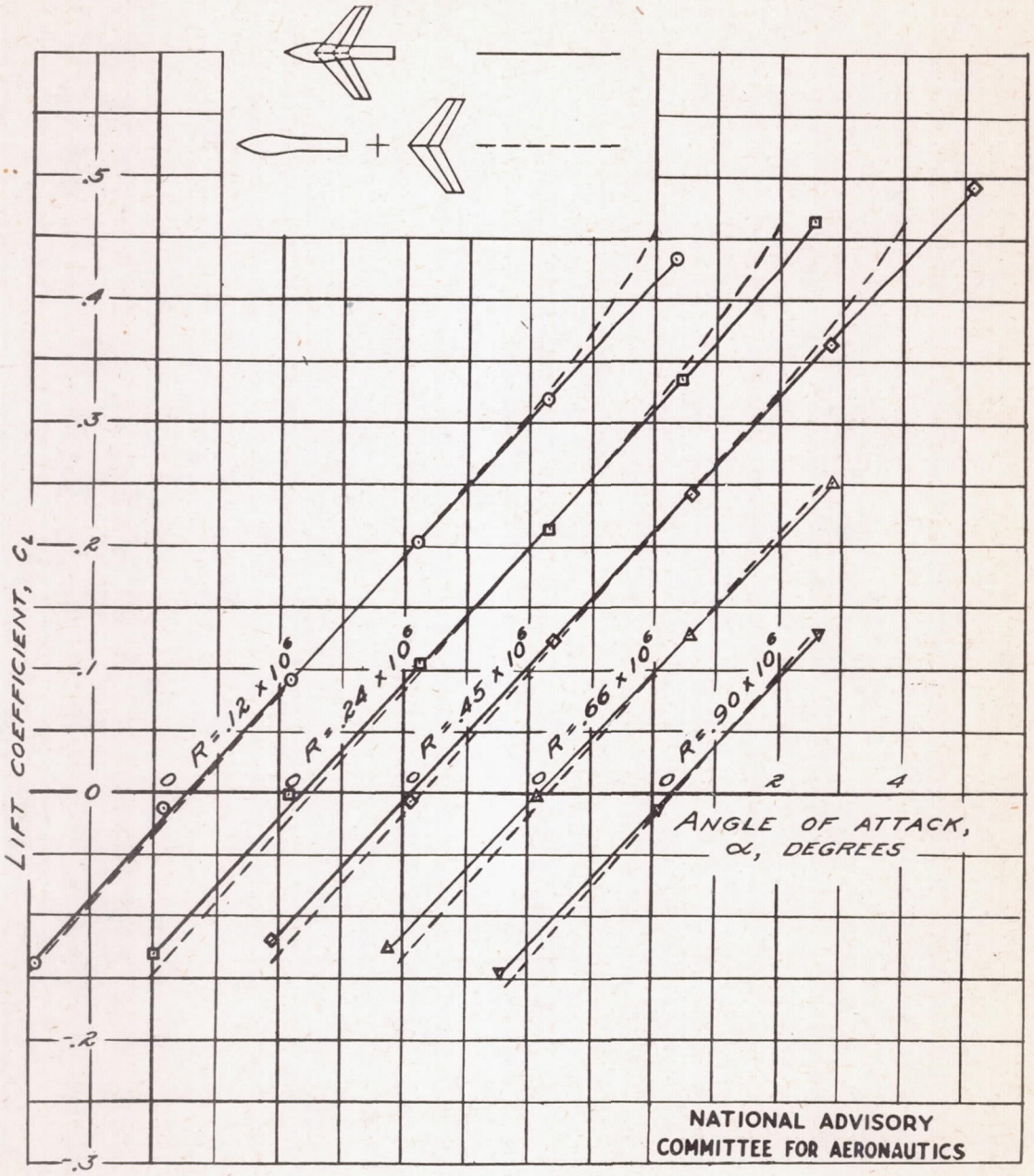

(f) Bulbous body, sweptback wing planform.

Figure 22. - Concluded.

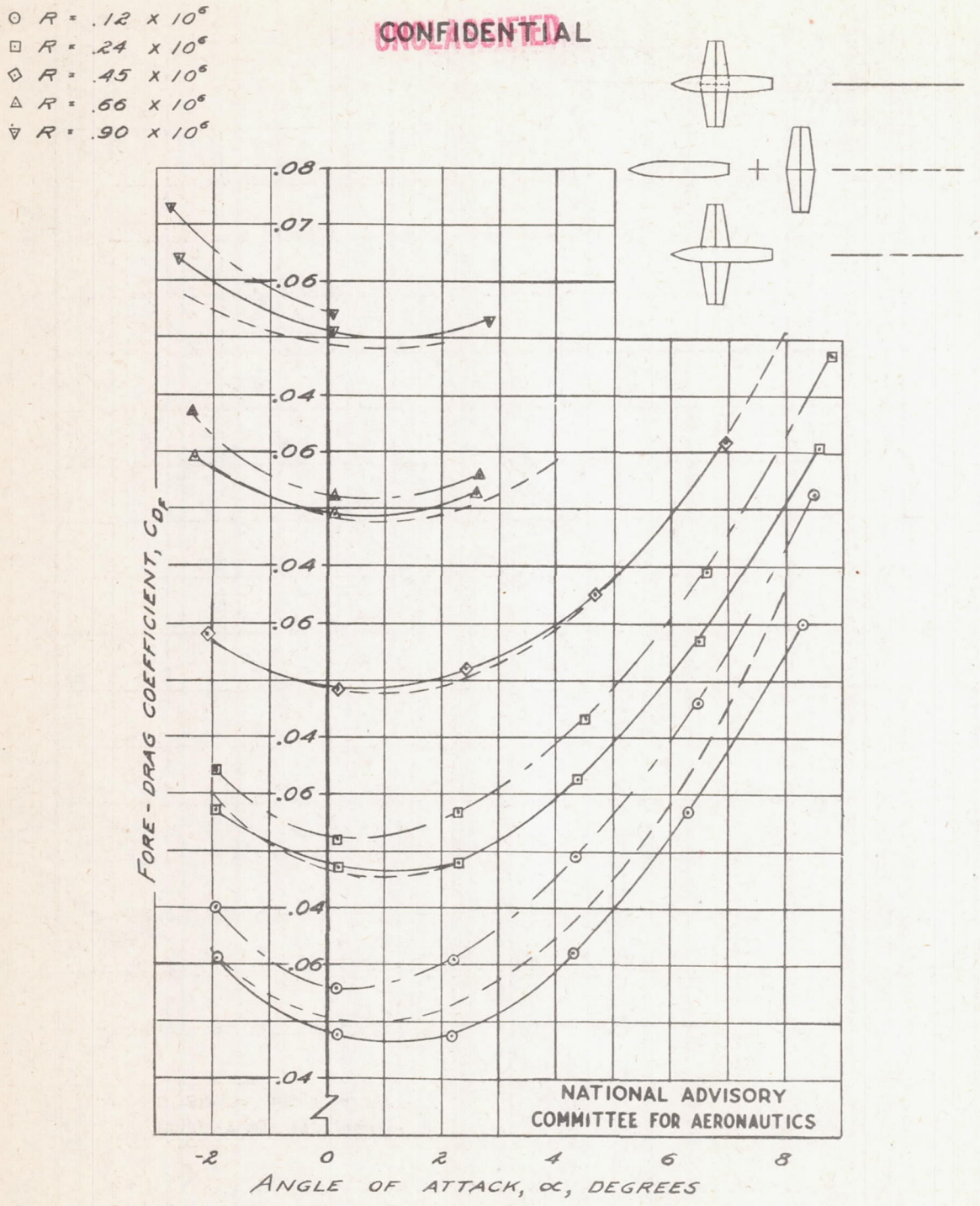

(a) BASIC BODY, STRAIGHT WING PLANFORM.

FIGURE 23. - FORE DRAGS OF WING-BODY COMBINATIONS COMPARED WITH SUM OF FORE DRAGS FOR COMPONENTS.

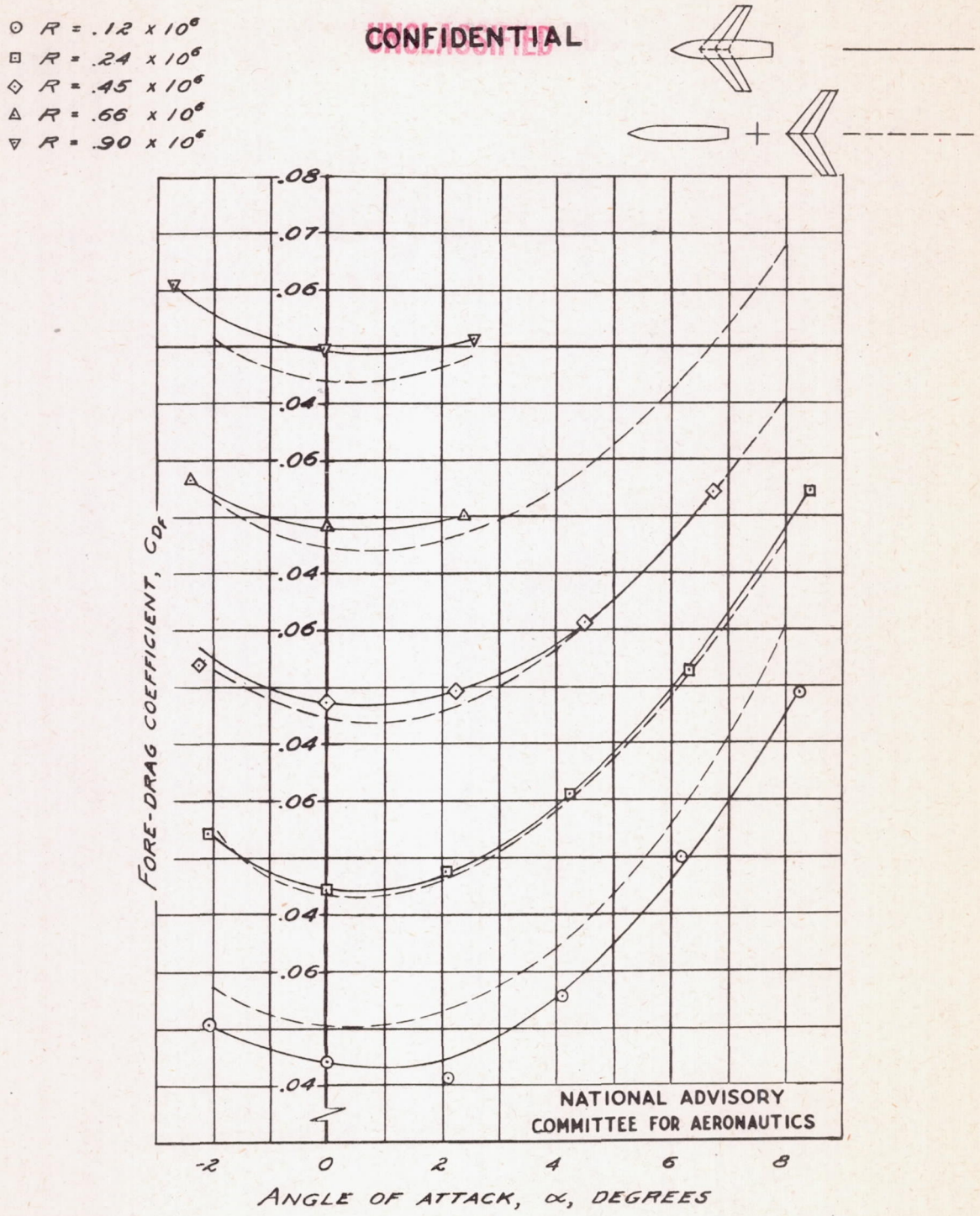

(b) BASIC BODY, SWEPTBACK WING PLANFORM.

FIGURE 23. - CONTINUED.

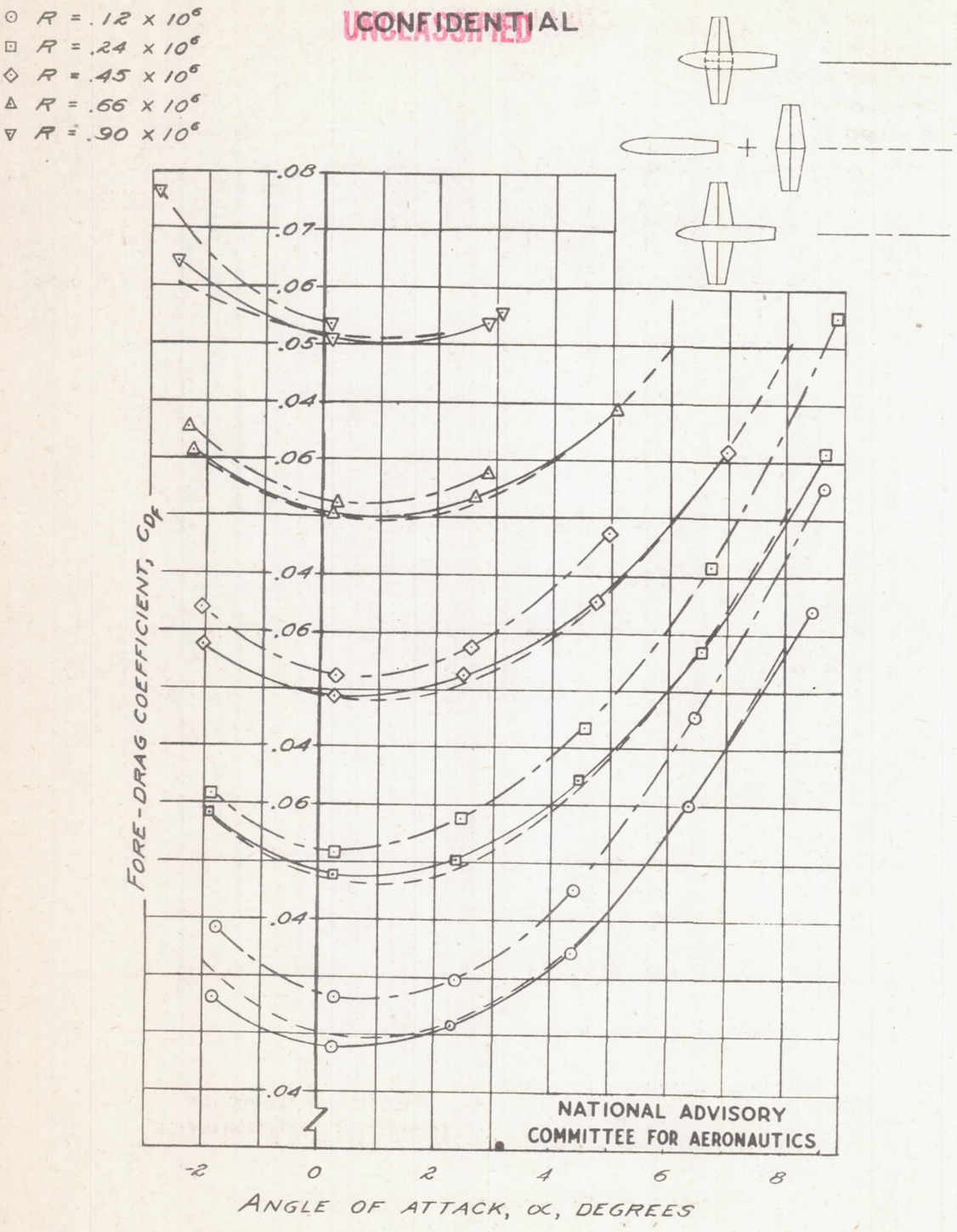

(c) BLUNT BODY, STRAIGHT WING PLANFORM.

FIGURE 23. - CONTINUED.

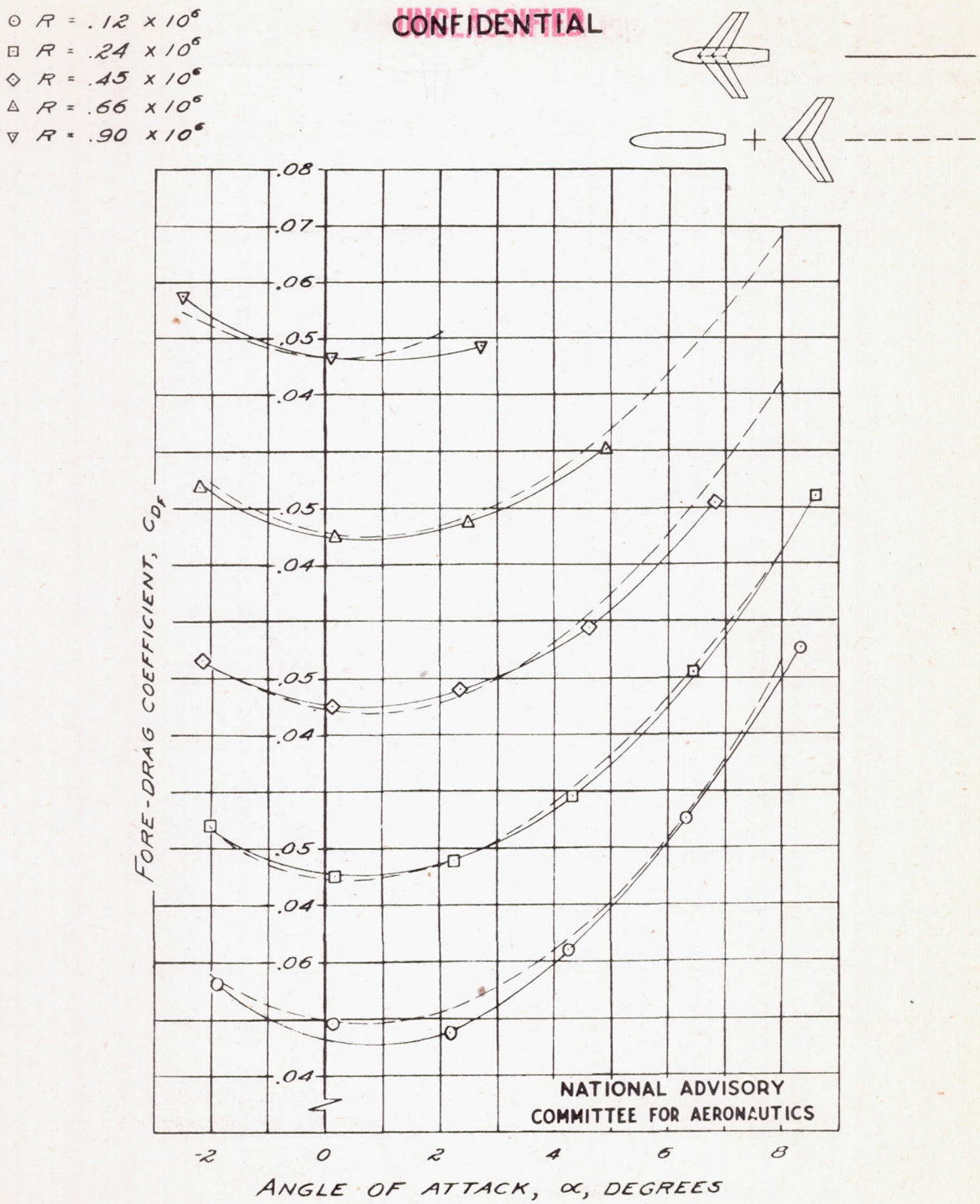

(d) BLUNT BODY, SWEPTBACK WING PLANFORM

FIGURE 23. - CONTINUED

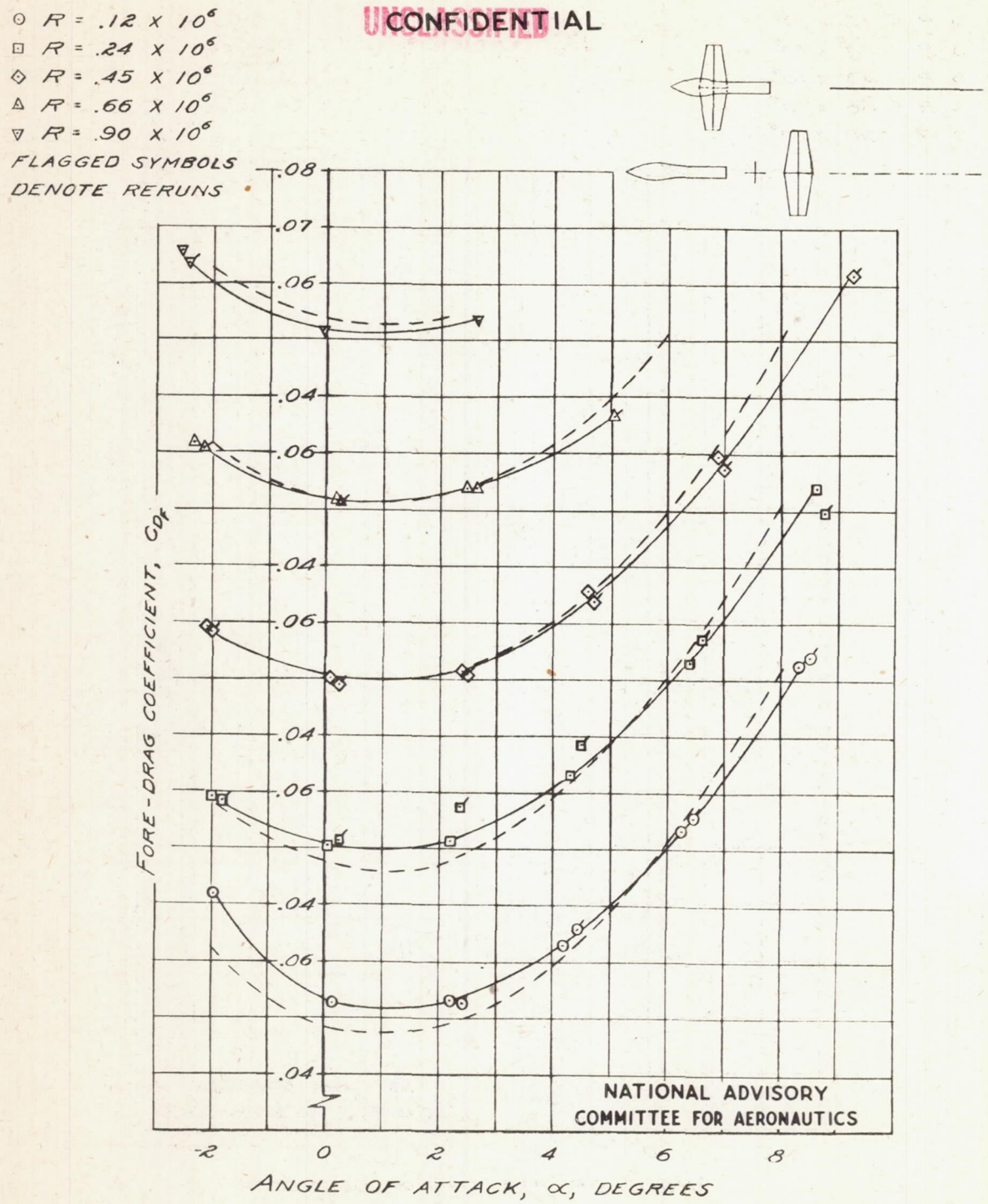

(e) Bulbous body, straight wing planform.

FIGURE 23. - CONTINUED

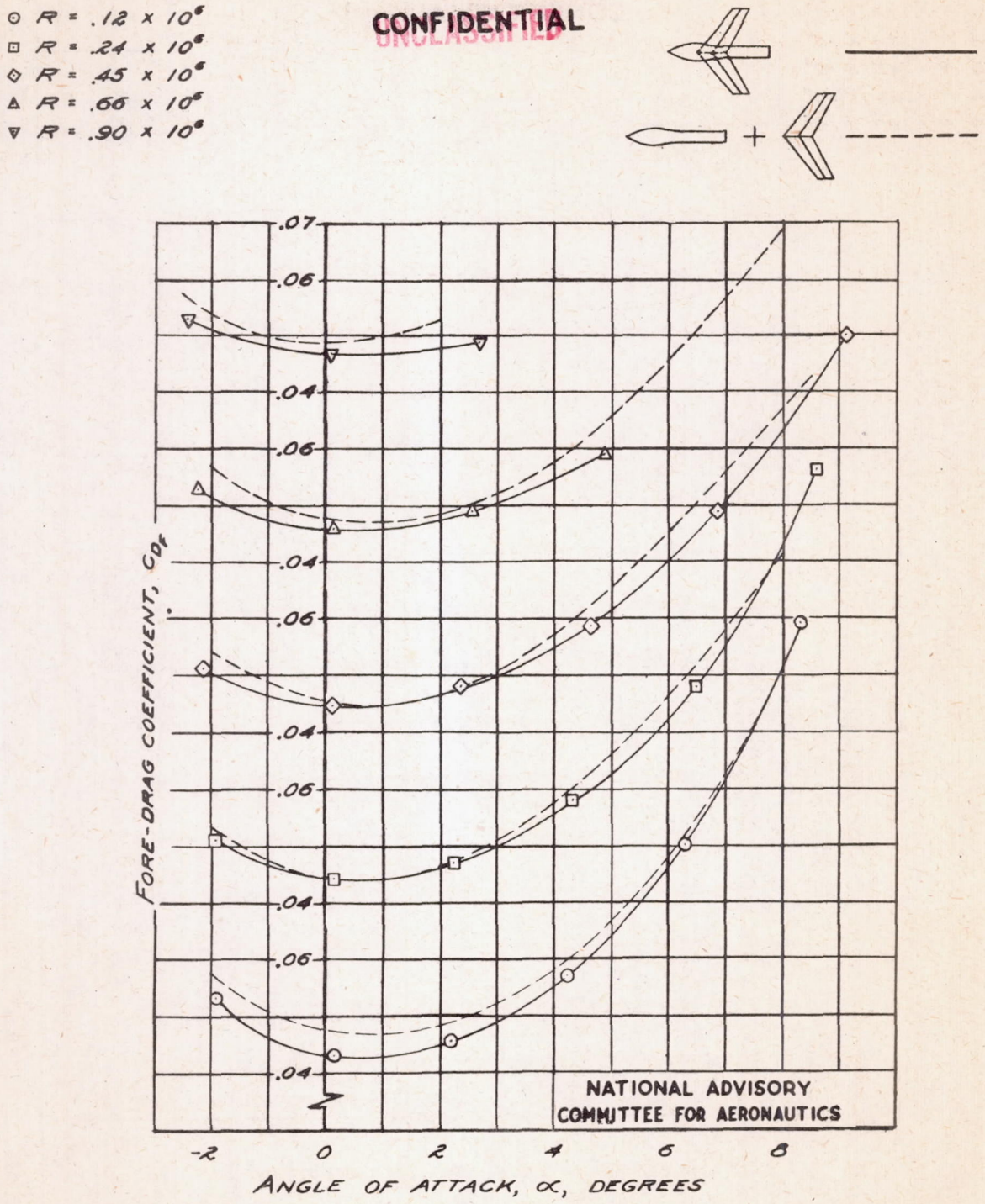

(f) BULBOUS BODY, SWEPTBACK WING PLANFORM.

FIGURE 23. - CONCLUDED.

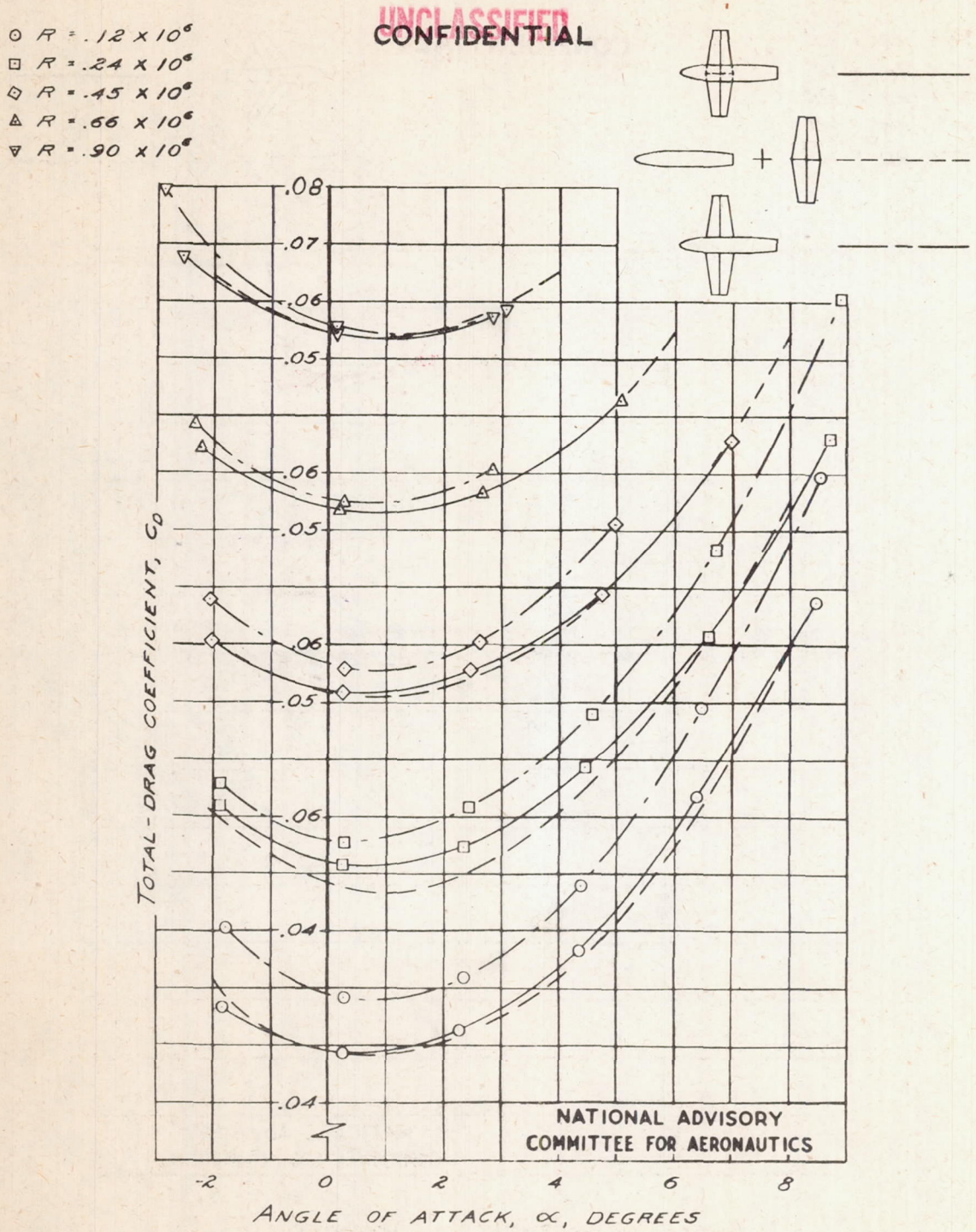

FIGURE 24. - TOTAL DRAGS FOR COMBINATIONS OF BLUNT BODY AND STRAIGHT WING PLANFORM COMPARED WITH SUM FOR COMPONENTS